Quantitative fluorescence photoacoustic tomography

Kui Ren* Hongkai Zhao†

March 6, 2013

Abstract

Fluorescence photoacoustic tomography (fPAT) is a multi-modality biomedical imaging technique that combines the high-resolution ultrasound imaging with the high-contrast fluorescence optical tomography. In the first step of fPAT, one utilizes the photoacoustic effect to recover the total absorbed energy map inside the media with ultrasound tomography. In the second step, called quantitative fPAT (QfPAT), one uses interior absorbed energy data to recover either the quantum efficiency or the concentration distribution or both of the fluorophores inside the media. The objective of this work is to derive the mathematical model for QfPAT and to study the corresponding inverse problems. We derive some uniqueness and stability results on these inverse problems, and propose a few (often explicit) reconstruction algorithms. Numerical simulations based on synthetic data are presented to verify the theory and algorithms proposed.

Key words. Fluorescence optical tomography, photoacoustic tomography, hybrid inverse problems, system of diffusion equations, interior data, quantitative fluorescence photoacoustic tomography.

AMS subject classifications 2010. 49N45, 65M32, 74J25, 92C55.

1 Introduction

Fluorescence optical tomography (FOT) is a molecular imaging technique in which fluorescent biochemical markers are injected into biological objects. The markers will then accumulate on targeted tissues, for instance cancer tissues, and emit near-infrared light (at wavelength λ_m) upon excitation by an external light source (at a different wavelength which we denote by λ_x). The objective of FOT is to determine the spatial concentration, lifetime distribution as well as quantum efficiency of the fluorophores inside the tissues from measured photon current data on the surface of the tissues. The information on the concentration, lifetime and quantum efficiency distributions of the fluorophores serve as diagnostic tools to differentiate healthy and cancerous tissues. We refer interested reader to [27, 48, 49, 71, 87] for overviews of fluorescence optical tomography.

*Department of Mathematics, University of Texas at Austin, Austin, TX 78712; ren@math.utexas.edu .
†Department of Mathematics, University of California, Irvine, CA 92697; zhao@math.uci.edu .

Besides the rapid advances in experimental design of disease-specific fluorescent markers, the field of FOT has witnessed tremendous development in image reconstruction techniques. Roughly speaking, image reconstructions in FOT are based on three types of measured data: steady-state (also known as continuous-wave) measurements [34, 37, 36, 54, 62, 88, 91], time-domain measurements [3, 25, 47, 50, 55, 73, 82, 85] and frequency-domain measurements [10, 23, 58, 59, 67, 75, 81, 89, 104]. In principle, steady-state measurements do not contain information on fluorescence lifetime while time-domain and frequency-domain measurements contain both the lifetime and fluorescence distribution information, even though time-domain data are significantly more difficult to measure in experiments [105, 112].

The major problem with FOT is the lack of stability [54, 73] of the imaging problem due to multiple scattering of light in biological tissues. The spatial resolution of the images reconstructed from experimental data is in general very low, even when multispectral and temperature-modulated data are used [24, 77]. To stabilize the imaging problem, several advanced reconstruction techniques have been designed in specific situations [35, 38, 40, 43, 102], and different types of *a priori* information have been proposed to be incorporated in reconstructions algorithms [76].

We propose in this work a new strategy to stabilize the FOT inverse problem: to combine fluorescence optical tomography with the high-resolution ultrasound tomography using the fluorescence photoacoustic effect. We call this new approach fluorescence photoacoustic tomography (fPAT). The physical principle of fPAT is identical to photoacoustic tomography (PAT) [5, 11, 20, 33, 63, 65, 74, 92, 114, 115, 118] except that in fPAT part of the ultrasound signal are generated from the fluorescent light. The objective of this work is to derive the mathematical model for fPAT as well as to present mathematical theory and reconstruction algorithms on the inverse problems involved. We point out that there have been several experimental work on using PAT to imaging fluorescent proteins [21, 95, 96, 113, 116], from slightly different perspectives.

The rest of the paper is organized as follows. We review in Section 2 the mathematical model for classical fluorescence optical tomography and derive the mathematical models for fPAT. We then study in detail uniqueness and stability issues for some inverse problems in quantitative fPAT (QfPAT) in Section 3. In Section 4 we present a general reconstruction algorithm for the numerical solution of the full nonlinear inverse problem of simultaneous reconstruction of quantum efficiency and fluorescence absorption coefficient (and thus fluorescence concentration). We then present some numerical simulations based on synthetic data in Section 5 to validate the theory and the algorithms we proposed. Concluding remarks are offered in Section 6.

2 Mathematical formulation

To study fluorescence photoacoustic tomography, we have to model the propagation of both excitation light and emission light. We denote by $\Omega \subset \mathbb{R}^d$ $(d = 2, 3)$ the tissue we plan to probe, with smooth boundary $\partial\Omega$, and c the speed of light inside the tissue. It is then known that the evolution of the density of the excitation photons, $u_x(\mathbf{x}, t)$, and that of the emission photons, $u_m(\mathbf{x}, t)$, solve the following system of coupled diffusion equations [3, 10,

25, 29, 47, 68, 79, 105]:

$$\begin{aligned}
\frac{1}{c}\frac{\partial u_x}{\partial t} - \nabla \cdot D_x(\mathbf{x})\nabla u_x(\mathbf{x},t) + \sigma_x(\mathbf{x})u_x(\mathbf{x},t) &= 0, && \text{in } \Omega \times \mathbb{R}_+ \\
\frac{1}{c}\frac{\partial u_m}{\partial t} - \nabla \cdot D_m(\mathbf{x})\nabla u_m(\mathbf{x},t) + \sigma_m(\mathbf{x})u_m(\mathbf{x},t) &= S(\mathbf{x},t), && \text{in } \Omega \times \mathbb{R}_+ \\
u_x(\mathbf{x},t) = g_x(\mathbf{x},t), \qquad u_m(\mathbf{x},t) &= 0, && \text{on } \partial\Omega \times \mathbb{R}_+ \\
u_x(\mathbf{x},t) = 0, \qquad u_m(\mathbf{x},t) &= 0, && \text{on } \Omega \times \{0\}
\end{aligned} \tag{1}$$

where the subscripts x and m denote the quantities at the excitation and emission wavelengths, respectively, and $g_x(\mathbf{x},t)$ is the external excitation source. The total absorption coefficient σ_x (resp. σ_m) consists of a contribution $\sigma_{x,i}$ (resp. $\sigma_{m,i}$) from the intrinsic tissue chromophores and a contribution $\sigma_{x,f}$ (resp. $\sigma_{m,f}$) from the fluorophores of the biochemical markers. It is generally believed in the FOT community that $\sigma_{m,f}$ is extremely small compared to the other coefficients so that it can be neglected in practice. We thus have

$$\sigma_x = \sigma_{x,i} + \sigma_{x,f}, \qquad \sigma_m = \sigma_{m,i} \tag{2}$$

in the rest of the paper. The fluorescence absorption coefficient $\sigma_{x,f}(\mathbf{x})$ is proportional to the concentration $\rho(\mathbf{x})$ and the extinction coefficient $\varepsilon(\mathbf{x})$ of the fluorophores, i.e. $\sigma_{x,f} = \varepsilon(\mathbf{x})\rho(\mathbf{x})$.

The emission source $S(\mathbf{x},t)$ generated at wavelength λ_m is mainly related to the fluorescence yield of the excitation. It can be expressed as

$$S(\mathbf{x},t) = \eta\sigma_{x,f}\Pi_\tau(u)(\mathbf{x},t) \equiv \eta\sigma_{x,f}\int_0^t \pi_\tau(t-s)u_x(\mathbf{x},s)ds \equiv \eta\sigma_{x,f}\int_0^t \frac{1}{\tau}e^{-\frac{(t-s)}{\tau}}u_x(\mathbf{x},s)ds \tag{3}$$

where $\eta(\mathbf{x})$ is called the quantum efficiency of the tissue. The product of the quantum efficiency and the fluorophores absorption coefficient, $\eta\sigma_{x,f}$, is called the quantum yield. The decay of the fluorescence follows an exponential law that is given by the kernel $\pi_\tau(t) = \frac{1}{\tau}e^{-\frac{t}{\tau}}$, where τ is the lifetime of the excited state. This model of emission source is considered in [3, 25, 68, 105] and in [10, 29, 47, 79] in the frequency-domain. It is often the model used to image lifetime of fluorophores.

In the propagation process, both the excitation light and the fluorescence light can be absorbed by the tissue. The total energy absorbed at location $\mathbf{x}$ and time t is [42]

$$\mathfrak{H}(\mathbf{x},t) = \sigma_x(\mathbf{x})u_x(\mathbf{x},t) + \sigma_m(\mathbf{x})u_m(\mathbf{x},t). \tag{4}$$

The absorbed energy then heats up the tissue to generate thermal expansion. Thermal expansions leads to a pressure field inside the tissue. This process is called the photoacoustic effect, or in our case called the fluorescence photoacoustic effect, and the resulted pressure field then evolves according to the acoustic wave equation [13, 18, 42]:

$$\begin{aligned}
\frac{1}{c_s^2(\mathbf{x})}\frac{\partial^2 p}{\partial t^2} - \Delta p &= \Xi\frac{\partial \mathfrak{H}}{\partial t}, && \text{in } \mathbb{R}^d \times \mathbb{R}_+ \\
p(\mathbf{x},t) = 0, \quad \frac{\partial p}{\partial t}(\mathbf{x},t) &= 0, && \text{in } \mathbb{R}^d \times \{0\}.
\end{aligned} \tag{5}$$

where $c_s(\mathbf{x})$ is the speed of ultrasound inside the tissue, and $\Xi(\mathbf{x})$ is the (*nondimensional*) Grüneisen coefficient that measures the photoacoustic efficiency of the underlying media [30, 33, 103]. Note that it is assumed here that the boundary of the domain has no effect on the propagation of the ultrasound, so that the acoustic wave equation is posed in $\mathbb{R}^d$, not Ω.

There are a few time scales in the physical processes we described above. The light absorption time scale $\tau_a \sim \frac{1}{c\sigma_x} \sim \frac{1}{c\sigma_m}$, the fluorescence decaying time scale τ, and the acoustic transport time scale: $\tau_{c_s} \sim \frac{\text{diam}(\Omega)}{c_s}$, diam$(\Omega)$ being diameter of the domain Ω. Due to the fact that the speed of light is significantly larger than the speed of the ultrasound, $c \gg c_s$, the light propagation process occurs on a much faster time scale than the acoustic wave propagation process: $\tau_{c_s} \gg \tau_a \sim \tau$. It is argued in [13, 18] with asympototic analysis that due to this scale separation between the acoustic and optical process, the term $\Xi\dfrac{\partial \mathfrak{H}}{\partial t}$ can be replaced with $H(\mathbf{x})\delta(t)$ where $H(\mathbf{x})$ is the time average of $\Xi(\mathbf{x})\mathfrak{H}(\mathbf{x},t)$:

$$H(\mathbf{x}) = \Xi(\mathbf{x})\big[\sigma_x(\mathbf{x})u_x(\mathbf{x}) + \sigma_m(\mathbf{x})u_m(\mathbf{x})\big]. \tag{6}$$

Here we abuse the notation a bit by introducing $u_x(\mathbf{x}) = \int_{\mathbb{R}_+} u_x(\mathbf{x},t)dt$ and $u_m(\mathbf{x}) = \int_{\mathbb{R}_+} u_m(\mathbf{x},t)dt$.

To derive a closed system of equations for $u_x(\mathbf{x})$ and $u_m(\mathbf{x})$, we integrate the system (1) with respect to time, and use the initial conditions and the fact that $u_x(\mathbf{x},\infty) = u_m(\mathbf{x},\infty) = 0$, to get

$$\begin{array}{rcll} -\nabla\cdot D_x(\mathbf{x})\nabla u_x(\mathbf{x}) + \sigma_x(\mathbf{x})u_x(\mathbf{x}) &=& 0, & \text{in } \Omega \\ -\nabla\cdot D_m(\mathbf{x})\nabla u_m(\mathbf{x}) + \sigma_m(\mathbf{x})u_m(\mathbf{x}) &=& \eta\sigma_{x,f}(\mathbf{x})v_x(\mathbf{x}), & \text{in } \Omega \\ u_x(\mathbf{x}) = g_x(\mathbf{x}), \qquad u_m(\mathbf{x}) &=& 0, & \text{on } \partial\Omega \end{array} \tag{7}$$

where we have introduced an auxiliary variable $v_x = \int_{\mathbb{R}_+} \Pi_\tau(u_x)(\mathbf{x},t)\ dt$.

Using the initial condition for $u_x(\mathbf{x},t)$, we can verify through integration by part that

$$\begin{aligned} \int_{\mathbb{R}_+}\int_0^t \frac{1}{c}\frac{\partial u_x}{\partial s}\frac{1}{\tau}e^{-\frac{t-s}{\tau}}dsdt &= \int_{\mathbb{R}_+}\big[\frac{1}{c\tau}u_x(\mathbf{x},s)e^{-\frac{t-s}{\tau}}|_0^t - \frac{1}{c\tau}\int_0^t \frac{1}{\tau}u_x(\mathbf{x},s)e^{-\frac{t-s}{\tau}}ds\big]dt \\ &= \frac{1}{c\tau}u_x(\mathbf{x}) - \frac{1}{c\tau}v_x(\mathbf{x}). \end{aligned} \tag{8}$$

We now convolve the equation for $u_x(\mathbf{x},t)$ in (1) with the kernel $\pi_\tau(t)$, integrate over time and use (8) to obtain an equation that couples u_x and v_x

$$-\nabla\cdot D_x(\mathbf{x})\nabla v_x(\mathbf{x}) + (\sigma_x(\mathbf{x}) - \frac{1}{c\tau})v_x(\mathbf{x}) = -\frac{1}{c\tau}u_x(\mathbf{x}), \ \text{ in } \Omega, \qquad v_x(\mathbf{x}) = g_x(\mathbf{x}), \ \text{ on } \partial\Omega. \tag{9}$$

Here we assumed that we can select $g(\mathbf{x},t)$ such that $\int_{\mathbb{R}_+} g_x(\mathbf{x},t)\ dt = \int_{\mathbb{R}_+} \Pi_\tau(g_x)(\mathbf{x},t)\ dt = g_x(\mathbf{x})$. This is clearly possible. For instance we can take $g_x(\mathbf{x},t) = g_x(\mathbf{x})\delta(t-0_+)$.

If we subtract the first equation in (7) from (9) and denote by $w_x = v_x - u_x$, we obtain the following equation for w_x:

$$-\nabla\cdot D_x(\mathbf{x})\nabla w_x(\mathbf{x}) + (\sigma_x(\mathbf{x}) - \frac{1}{c\tau})w_x(\mathbf{x}) = 0, \ \text{ in } \Omega, \qquad w_x(\mathbf{x}) = 0, \ \text{ on } \partial\Omega. \tag{10}$$

If $q(\mathbf{x}) \equiv \sigma_x(\mathbf{x}) - \dfrac{1}{c\tau} > 0$ a.e. (which means that the lifetime of the fluorophore is greater than the absorption time scale $\dfrac{1}{c\sigma_x}$), $w_x = 0$ a.e.. Otherwise, if Ω is such that 0 is *not* an eigenvalue of the operator $\nabla \cdot D_x \nabla - q$ with homogeneous Dirichlet boundary condition, we have $w_x = 0$ a.e.. In both cases, we have $v_x(\mathbf{x}) = u_x(\mathbf{x})$ a.e..

We now have the following system of diffusion equations for $u_x(\mathbf{x})$ and $u_m(\mathbf{x})$:

$$\begin{array}{rcll} -\nabla \cdot D_x(\mathbf{x})\nabla u_x(\mathbf{x}) + \sigma_x(\mathbf{x})u_x(\mathbf{x}) &=& 0, & \text{in } \Omega \\ -\nabla \cdot D_m(\mathbf{x})\nabla u_m(\mathbf{x}) + \sigma_m(\mathbf{x})u_m(\mathbf{x}) &=& \eta\sigma_{x,f}(\mathbf{x})u_x(\mathbf{x}), & \text{in } \Omega \\ u_x(\mathbf{x}) = g_x(\mathbf{x}), \quad u_m(\mathbf{x}) &=& 0, & \text{on } \partial\Omega \end{array} \tag{11}$$

For the convenience of the presentation at times, we denote by $A^{i,j}_{\alpha,\beta}$ ($\alpha, \beta \in \{x, m\}$) the diffusion coefficient matrix and $a_{\alpha\beta}$ the absorption coefficient matrix. Then we can write down this system as:

$$-\mathcal{D}_i[A^{ij}_{\alpha\beta}\mathcal{D}_j u_\beta] + a_{\alpha\beta}u_\beta = f_\alpha, \quad \text{in } \Omega, \qquad u_\alpha = g_\alpha, \quad \text{on } \partial\Omega. \tag{12}$$

with

$$A^{ij}_{\alpha\alpha} = D_\alpha \delta_{ij}, \qquad A^{ij}_{\alpha\beta} = 0 \ \text{ if } \ \alpha \neq \beta, \qquad f_\alpha = 0 \tag{13}$$

$$(a_{\alpha\beta}) = \begin{pmatrix} \sigma_x & 0 \\ -\eta\sigma_{x,f} & \sigma_m \end{pmatrix}, \qquad g_\alpha = \begin{cases} g_x, & \alpha = x \\ 0, & \alpha = m \end{cases} \tag{14}$$

Note that because $(a_{\alpha\beta})$ is not symmetric, the system (11) is not self-adjoint.

Throughout the paper, we denote by $\mathcal{H}^k(\Omega)$ the space of functions whose derivatives of order less than k are in $L^2(\Omega)$. We assume that:

(**A-i**) The domain Ω is simply-connected with C^2 boundary $\partial\Omega$. The optical coefficients $(D_x, \sigma_{x,i}) \in C^1(\bar{\Omega}) \times L^\infty(\Omega)$, $(D_m, \sigma_m) \in C^1(\bar{\Omega}) \times L^\infty(\Omega)$, $\sigma_{x,f}, \eta, \Xi \in L^\infty(\Omega)$ and $0 < c_0 \leq D_x, \sigma_{x,i}, D_m, \sigma_m, \eta, \sigma_{x,f}, \Xi \leq C_0 < \infty$ for some positive c_0 and C_0. The illumination $g_x(\mathbf{x})$ is the restriction of a $C^2(\bar{\Omega})$ function on $\partial\Omega$ and $g_x(\mathbf{x})$ is positive, $g_x \geq \tilde{c}_0 > 0$ for some $\tilde{c}_0$.

With these assumptions, it is straightforward to verify that $A^{ij}_{\alpha\beta}$ satisfies the strong Legendre condition and the system (12) is thus strongly elliptic [70, 80]. In fact, this system admits a unique solution following standard elliptic theory [41, 46, 70, 80].

Lemma 2.1. *Assume that the coefficients and the domain satisfies the regularity assumptions in (***A-i***). Then system* (11) *admits a unique solution* (u_x, u_m)*, positive a.e., of class* $\mathcal{H}^2(\Omega) \times \mathcal{H}^2(\Omega)$.

Proof. We conclude from the first equation in (11) and its boundary condition that there is a unique solution $u_x \in \mathcal{H}^2(\Omega)$ [41, 46], positive a.e.. This implies that $\eta\sigma_{x,f}u_x \in L^\infty(\Omega)$. We then conclude from the second equation that there is a unique solution $u_m \in \mathcal{H}^2(\Omega)$, positive a.e. inside Ω. □

Remark 2.2. The regularity of solutions of (11) implies that the data function $H(\mathbf{x})$ defined in (6) lies in $L^\infty(\Omega)$. For the theory in the rest of the paper to work, we can relax slightly some of the assumptions we made on the coefficients. We will not worry about this technical detail here.

3 The inverse problem

We are now ready to formulate the inverse problem in fluorescence photoacoustic tomography. That is, to reconstruct the set of parameters $D_x, D_m, \sigma_{x,i}, \sigma_m, \Xi, \eta$ and $\sigma_{x,f}$ in (11) and (6) from measured acoustic data (for time that is long enough, say, $t_{\max}$) collected from different excitations, i.e. the map:

$$\Lambda_{D_x,D_m,\sigma_{x,i},\sigma_m,\Xi,\eta,\sigma_{x,f}} : g_x(\mathbf{x}) \mapsto p(\mathbf{x},t)_{|\partial\Omega\times(0,t_{\max})}. \tag{15}$$

This problem can be solved in two steps in sequence. In the first step, we reconstruct the initial pressure field $H(\mathbf{x})$ in (6) from acoustic pressure data $p(\mathbf{x},t)_{|\partial\Omega\times(0,t_{\max})}$. This step has been thoroughly studied in the past a few years; see for instance [2, 4, 8, 9, 22, 32, 39, 51, 52, 53, 56, 57, 61, 64, 69, 83, 84, 94, 90, 92, 93, 106, 107, 108, 109, 110, 111, 117, 119, 120] and references therein. The second step, which we called quantitative fPAT (QfPAT), is to reconstruct the coefficients $D_x, D_m, \sigma_{x,i}, \sigma_m, \Xi, \eta$ and $\sigma_{x,f}$ from interior data $H(\mathbf{x})$ that we obtained from the first step.

In this work, we assume that the fist step of fPAT has been done already so that we are now given the interior data (6). We assume also that:

(**A-ii**) The coefficients (D_x, $\sigma_{x,i}$) are reconstructed at the excitation wavelength before the markers are injected, with a quantitative PAT step as those in [6, 7, 13, 14, 15, 18, 19, 30, 31, 44, 45, 72, 78, 99, 100, 101, 103, 123]. The coefficients (D_m, σ_m) are reconstructed at the emission wavelength after the markers are injected (but before the fluorophores are excited) with another quantitative PAT step. The Grüneisen coefficient Ξ is known as well, for instance by a multi-spectral quantitative PAT step as in [16].

We observe that $\sigma_{x,f}$ can not be known in advance because markers have to be injected into the tissue before one can measure $\sigma_{x,f}$. Once markers are injected, any illumination at the excitation wavelength would excite the markers and thus the light from emission wavelength appears in the domain. Our main objective is thus to reconstruct the absorption coefficient $\sigma_{x,f}$ and the quantum efficiency η in the system (11) from the data $H(\mathbf{x})$ in (6).

3.1 Reconstructing η

We now consider the problem of reconstructing the quantum efficiency η assuming that the fluorophore absorption coefficient $\sigma_{x,f}$ is known. We observe that this is a linear inverse problem. Moreover, we have a unique and stable way to reconstruct the unknown as stated below.

Proposition 3.1. *Let H and $\tilde{H}$ be two data sets generated from (11) in the form of (6) with coefficients ($\sigma_{x,f}$, η) and ($\sigma_{x,f}$, $\tilde{\eta}$) respectively. Then $H = \tilde{H}$ implies $\eta = \tilde{\eta}$. Moreover,*

$$c_1 \|\frac{H-\tilde{H}}{\Xi\sigma_m}\|_{\mathcal{H}^2(\Omega)} \leq \|(\eta-\tilde{\eta})u_x\|_{L^2(\Omega)} \leq c_2 \|\frac{H-\tilde{H}}{\Xi\sigma_m}\|_{\mathcal{H}^2(\Omega)} \tag{16}$$

with c_1, c_2 constants that depend on Ω, D_m, σ_m and $\sigma_{x,f}$.

Proof. Let $(u_x,\ u_m)$ and $(\tilde{u}_x,\ \tilde{u}_m)$ be the solution of (11). Then it is straightforward to see from the first equation that $u_x = \tilde{u}_x$. Together with $H = \tilde{H}$ this implies $u_m = \tilde{u}_m$. The second equation then implies $\eta = \tilde{\eta}$. To derive the stability estimate, let us denote by $w_x = u_x - \tilde{u}_x$ and $w_m = u_m - \tilde{u}_m$. It is straightforward to check that $w_x = 0$ and w_m solves the following equation

$$-\nabla \cdot D_m \nabla w_m + \sigma_m w_m = (\eta - \tilde{\eta})\sigma_{x,f} u_x, \quad \text{in } \Omega, \qquad w_m = 0, \quad \text{on } \partial\Omega. \tag{17}$$

We also verify that

$$w_m = \big(H - \tilde{H}\big)/(\Xi\sigma_m). \tag{18}$$

The equation on the left then follows directly from standard elliptic stability estimate of equation (17) [41, 46], (18) and the fact that $\sigma_{x,f}$ is bounded from above. From (17) and the fact that $\sigma_{x,f}$ is bounded from below, we conclude that

$$\begin{aligned} &|(\eta - \tilde{\eta})u_x|^2 \le \tilde{c}(|\nabla \cdot D_m \nabla w_m|^2 + |\sigma_m w_m|^2) = \tilde{c}(|\nabla \cdot D_m \nabla \frac{\sigma_m w_m}{\sigma_m}|^2 + |\sigma_m w_m|^2) \\ &\le \tilde{\tilde{c}}(|\frac{D_m}{\sigma_m}\Delta(\sigma_m w_m)|^2 + |\big(\nabla \frac{D_m}{\sigma_m} + D_m \nabla \frac{1}{\sigma_m}\big) \cdot \nabla(\sigma_m w_m)|^2 + (1 + |\nabla \cdot D_m \nabla \frac{1}{\sigma_m}|^2)|\sigma_m w_m|^2). \end{aligned} \tag{19}$$

The stability result (16) then follows from (19), (18) and the regularity and boundedness assumptions on the coefficients D_m and σ_m, Ξ given in (**A-i**). □

This result shows that we can uniquely reconstruct η from one interior data H. In the reconstruction process, however, we have to differentiate the data twice. We thus lose exactly two derivatives. Note that the weight u_x in the estimate does *not* depend on the unknown to be reconstructed. The argument in the proof also provides an explicit reconstruction algorithm for recovering η. The algorithm works as follows.

Algorithm I: To reconstructing η.

S1. Given σ_x, solve the first equation in the system (11) (with the boundary condition) for u_x;

S2. Subtract $\sigma_x u_x$ from H/Ξ and divide the result by σ_m to obtain u_m;

S3. Reconstruct η as $\big(-\nabla \cdot D_m \nabla u_m + \sigma_m u_m\big)/\big(\sigma_{x,f} u_x\big)$.

3.2 Reconstructing $\sigma_{x,f}$

We now study the problem of reconstructing $\sigma_{x,f}$ assuming that η is known. This is a nonlinear inverse problem.

Linearized case. We first consider a special linearized model that is often used in fluorescence optical tomography, such as in [91]. In this model, it is assumed that $\sigma_{x,f} \ll \sigma_{xi}$ (which is indeed the case in practical applications). It is thus reasonable to assume that the absorption coefficient σ_x in the first diffusion equation of (11) and in the data (6) is known and equals $\sigma_{x,i}$. We are thus only required to reconstruct the coefficient $\sigma_{x,f}$ in the

source term in the second equation of (11) assuming η is also known. The inverse problem in this case has exactly the same structure as the problem of reconstructing η as we just studied. In fact, we can derive a stability estimate that is identical to (16) for $\sigma_{x,f}$ and using the same reconstruction algorithm for η to reconstruct $\sigma_{x,f}$. Note that in this model, the coefficient η and $\sigma_{x,f}$ only appear in the equation as the product $\eta\sigma_{x,f}$. It is thus not possible to reconstruct separately the two coefficients, but only their product.

Nonlinear case. To study the nonlinear problem, we first re-write the PDE system slightly using the data H. Precisely, we add $-\sigma_x u_x - \sigma_m u_m$ to the left-hand-side of the first equation and $-H/\Xi$ to the right-hand-side of the first equation, and then add $\eta(\sigma_x u_x + \sigma_m u_m)$ to the left-hand-side of the second equation and $\eta H/\Xi$ to the right-hand-side of the second equation. We obtain, after slight re-arrangement, the following system of equations:

$$\begin{aligned} -\nabla\cdot D_x(\mathbf{x})\nabla u_x(\mathbf{x}) - \sigma_m u_m &= -H/\Xi, \quad \text{in } \Omega \\ -\nabla\cdot D_m(\mathbf{x})\nabla u_m(\mathbf{x}) + (\eta+1)\sigma_m u_m + \eta\sigma_{x,i} u_x(\mathbf{x}) &= \eta H/\Xi, \quad \text{in } \Omega \\ u_x(\mathbf{x}) = g_x, \quad u_m(\mathbf{x}) &= 0, \quad \text{on } \partial\Omega \end{aligned} \tag{20}$$

This is a system of elliptic PDEs with all coefficients *known*. We can write the system into the form of (12) with

$$A^{ij}_{xx} = D_x\delta_{ij}, \quad A^{ij}_{mm} = D_m\delta_{ij}, \quad A^{ij}_{xm} = A^{ij}_{mx} = 0 \tag{21}$$

$$(a_{\alpha\beta}) = \begin{pmatrix} 0 & -\sigma_m \\ \eta\sigma_{x,i} & (\eta+1)\sigma_m \end{pmatrix}, \quad f_\alpha = \begin{cases} -H/\Xi, & \alpha = x \\ \eta H/\Xi, & \alpha = m \end{cases}, \qquad g_\alpha = \begin{cases} g_x, & \alpha = x \\ 0, & \alpha = m \end{cases}. \tag{22}$$

We write the corresponding homogeneous boundary value problem as

$$-\mathcal{D}_i[A^{ij}_{\alpha\beta}\mathcal{D}_j u_\beta] + a_{\alpha\beta}u_\beta = 0, \quad \text{in } \Omega, \qquad u_\alpha = 0, \quad \text{on } \partial\Omega, \qquad \alpha,\beta \in \{x, m\}. \tag{23}$$

We then have the following result on the inverse problem.

Theorem 3.2. *Let H and $\tilde{H}$ be two data sets generated from (11) in the form of (6) with coefficients $(\sigma_{x,f}, \eta)$ and $(\tilde{\sigma}_{x,f},\eta)$ respectively. Assume that the homogeneous problem (23) admits $\mathbf{0}$ as its only solution. Then $H = \tilde{H}$ implies $\sigma_{x,f} = \tilde{\sigma}_{x,f}$. Moreover,*

$$\|(\sigma_{x,f} - \tilde{\sigma}_{x,f})u_x\|_{L^2(\Omega)} \le c\|H - \tilde{H}\|_{L^2(\Omega)} \tag{24}$$

with c a constant that depends on Ω, D_x, $\sigma_{x,i}$, D_m, σ_m, η and Ξ.

Proof. Let (u_x, u_m) and $(\tilde{u}_x, \tilde{u}_m)$ be the solution of the system (12) with H and $\tilde{H}$ respectively. We verify that $(u_x - \tilde{u}_x, u_m - \tilde{u}_m)$ solves

$$-\mathcal{D}_i[A^{ij}_{\alpha\beta}\mathcal{D}_j(u_\beta - \tilde{u}_\beta)] + a_{\alpha\beta}(u_\beta - \tilde{u}_\beta) = (f_\alpha - \tilde{f}_\alpha), \quad \text{in } \Omega, \qquad u_\alpha - \tilde{u}_\alpha = 0, \quad \text{on } \partial\Omega. \tag{25}$$

By the assumption, the homogeneous problem (23) has only trivial solution $\mathbf{0}$. Fredholm alternative [70, 80] then ensures that there exists a unique solution to the boundary value

problem (25). We observe that $H = \tilde{H}$ implies $f_\alpha = \tilde{f}_\alpha$ ($\alpha = x, m$). This then implies $(u_x, u_m) = (\tilde{u}_x, \tilde{u}_m)$. Uniqueness of the inverse problem then follows from the fact that

$$(\sigma_{x,f} - \tilde{\sigma}_{x,f})u_x = (H - \tilde{H})/\Xi - \tilde{\sigma}_x(u_x - \tilde{u}_x) - \sigma_m(u_m - \tilde{u}_m). \tag{26}$$

To derive the stability result, we observe that, with the assumptions on the regularity of the coefficients in (**A-i**), the following stability estimate holds for the solution of (25) [70, 80]:

$$\|(u_x, u_m) - (\tilde{u}_x, \tilde{u}_m)\|_{[L^2(\Omega)]^2} \leq \tilde{c}_0 \|H - \tilde{H}\|_{L^2(\Omega)}. \tag{27}$$

where $\tilde{c}$ depends on Ω, D_x, $\sigma_{x,i}$, D_m, σ_m, η and Ξ. Meanwhile, identity (26) implies, using the fact that $\tilde{\sigma}_x$ and other coefficients are bounded, that,

$$\|(\sigma_{x,f} - \tilde{\sigma}_{x,f})u_x\|_{L^2(\Omega)} \leq \tilde{c}_1 \|H - \tilde{H}\|_{L^2(\Omega)} + \tilde{c}_2 \|(u_x, u_m) - (\tilde{u}_x, \tilde{u}_m)\|_{[L^2(\Omega)]^2}, \tag{28}$$

where $\tilde{\tilde{c}}_1$ depends on Ξ and $\tilde{\tilde{c}}_2$ depend on $\sigma_{x,i}$ and σ_m. The stability result (24) then follows from (27) and (28). □

The above result provides a reconstruction algorithm for the inverse problem when the system (20) admits a unique solution.

Algorithm II: To reconstructing $\sigma_{x,f}$.

S1. Given data H, solve (20) to recover (u_x, u_m);

S2. Reconstruct $\sigma_{x,f}$ as $\sigma_{x,f} = (H/\Xi - \sigma_m u_m)/u_x - \sigma_{x,i}$.

The above uniqueness of the solution to the inverse problem holds when system (20) is uniquely solvable, i.e., when the homogeneous problem (23) has only trivial solution $\mathbf{0}$. Since the differential operator $-\mathcal{D}_i[A^{ij}_{\alpha\beta}\mathcal{D}_j\,\cdot] + a_{\alpha\beta}\,\cdot$ (with Dirichlet boundary condition) is strongly elliptic, one expect that its kernel is finite-dimensional. In other words, system (20) is indeed uniquely solvable most of the times. We now show two cases where we know for sure that (23) has only trivial solution $\mathbf{0}$.

Proposition 3.3. *The homogeneous elliptic system* (23) *admits only trivial solution* $\mathbf{0}$ *if one of the following statement is true:*
(i) $\eta\sigma_{x,i} - \sigma_m = 0$*;*
(ii) $(\sigma_m, D_m) = \kappa(\sigma_{x,i}, D_x)$, $\kappa \neq 0$ *being a positive constant.*

Proof. When (i) holds, $a_{\alpha\beta}$ is positive-semidefinite (in the sense that $(\frac{a_{\alpha\beta}+a_{\beta\alpha}}{2})$ is positive semidefinite). The result then follows from Lax-Milgram theory [26, 46, 80]. When (ii) holds, we add the two equations in the system together to obtain

$$-\nabla \cdot D_x \nabla(u_x + \kappa u_m) + \eta\sigma_{x,i}(u_x + \kappa u_m) = 0, \quad \text{in} \quad \Omega, \quad u_x + \kappa u_m = 0, \quad \text{on} \quad \partial\Omega. \tag{29}$$

The assumption on the coefficients in (**A-i**) then implies that $u_x + \kappa u_m = 0$, and thus $u_m = -u_x/\kappa$. Using this relation in the first equation leads to

$$-\nabla \cdot D_x \nabla u_x + \frac{\sigma_m}{\kappa} u_x = 0, \quad \text{in} \quad \Omega, \quad u_x = 0, \quad \text{on} \quad \partial\Omega. \tag{30}$$

This in turn proves that $u_x = 0$. Thus $u_m = u_x = 0$. □

Remark 3.4. In most of the engineering literature, it is assumed that case (ii) is true with $\kappa = 1$. In fact, it is more realistic to assume that κ depends on the wavelengths λ_x and λ_m [28, 30, 33, 60, 72, 95, 97, 103, 121, 122]. The result holds as long as κ does not depend on the spatial variable $\mathbf{x}$.

3.3 Reconstructing η and $\sigma_{x,f}$

We now consider the reconstruction of the two parameters η and $\sigma_{x,f}$ simultaneously. We first observe that even though the inverse problem is linear with respect to η for a fixed $\sigma_{x,f}$, it is nonlinear when both coefficients are to be sought due to the existence of the product term $\eta\sigma_{x,f}$ in the elliptic system (11). In practical applications, it is generally assumed that the parameter $\sigma_{x,f}$ is significantly smaller than $\sigma_{x,i}$, $\sigma_{x,f} \ll \sigma_{x,i}$. It is thus often enough to consider the inverse problem partially linearized at $(\eta, 0)$. We observe that we can indeed linearize the inverse problem at any background.

Lemma 3.5. *The data H defined in (6), viewed as the map*

$$H[\eta,\sigma_{x,f}]: \begin{array}{ccc} (\eta,\sigma_{x,f}) & \mapsto & \Xi\big(\sigma_x u_x + \sigma_m u_m\big) \\ L^\infty(\Omega)\times L^\infty(\Omega) & \mapsto & L^\infty(\Omega) \end{array} \tag{31}$$

*is Fréchet differentiable at any $(\eta, \sigma_{x,f}) \in L^\infty(\Omega) \times L^\infty(\Omega)$ that satisfies the assumptions in (**A-i**). The derivative at $(\eta, \sigma_{x,f})$ is given by*

$$\begin{pmatrix} d_1 H[\eta,\sigma_{x,f}](\delta\eta) \\ d_2 H[\eta,\sigma_{x,f}](\delta\sigma_{x,f}) \end{pmatrix} = \Xi \begin{pmatrix} \sigma_m w_m \\ \delta\sigma_{x,f} u_x + \sigma_x v_x + \sigma_m v_m \end{pmatrix} \tag{32}$$

for $(\delta\eta, \delta\sigma_{x,f}) \in L^\infty(\Omega) \times L^\infty(\Omega)$, (v_x, v_m) the unique solution of

$$\begin{array}{rcll} -\nabla\cdot D_x(\mathbf{x})\nabla v_x(\mathbf{x}) + \sigma_x v_x(\mathbf{x}) &=& -\delta\sigma_{x,f} u_x, & \text{in } \Omega \\ -\nabla\cdot D_m(\mathbf{x})\nabla v_m(\mathbf{x}) + \sigma_m v_m(\mathbf{x}) &=& \eta\sigma_{x,f} v_x + \eta\delta\sigma_{x,f} u_x, & \text{in } \Omega \\ v_x(\mathbf{x}) = 0, \quad v_m(\mathbf{x}) &=& 0, & \text{on } \partial\Omega \end{array} \tag{33}$$

and w_m the unique solution of

$$-\nabla\cdot D_m(\mathbf{x})\nabla w_m(\mathbf{x}) + \sigma_m w_m(\mathbf{x}) = \delta\eta\sigma_{x,f} u_x, \quad \text{in } \Omega, \qquad w_m = 0, \quad \text{on } \partial\Omega. \tag{34}$$

Proof. By the chain rule and the product rule, it is clear from (6) that we only need to show that (u_x, u_m) is Fréchet differentiable with respect to each coefficient. We prove here the result with respect to $\sigma_{x,f}$. Let us denote by (u'_x, u'_m) the solution of (11) with coefficients $\sigma_{x,f} + \delta\sigma_{x,f}$, $\delta\sigma_{x,f} \in L^\infty(\Omega)$ with small norm $\|\delta\sigma_{x,f}\|_{L^\infty(\Omega)} \ll 1$, and $(\tilde{u}_x,\ \tilde{u}_m)=(u'_x - u_x,\ u'_m - u_m)$, $(\tilde{\tilde{u}}_x,\ \tilde{\tilde{u}}_m)=(u'_x - u_x - v_x,\ u'_m - u_m - v_m)$. It is then straightforward to verify that $(\tilde{u}_x,\ \tilde{u}_m)$ solves

$$\begin{array}{rcll} -\nabla\cdot D_x(\mathbf{x})\nabla\tilde{u}_x(\mathbf{x}) + (\sigma_x + \delta\sigma_{x,f})\tilde{u}_x(\mathbf{x}) &=& -\delta\sigma_{x,f} u_x, & \text{in } \Omega \\ -\nabla\cdot D_m(\mathbf{x})\nabla\tilde{u}_m(\mathbf{x}) + \sigma_m\tilde{u}_m(\mathbf{x}) &=& \eta(\sigma_{x,f} + \delta\sigma_{x,f})\tilde{u}_x + \eta\delta\sigma_{x,f} u_x, & \text{in } \Omega \\ \tilde{u}_x(\mathbf{x}) = 0, \quad \tilde{u}_m(\mathbf{x}) &=& 0, & \text{on } \partial\Omega. \end{array} \tag{35}$$

and $(\tilde{\tilde{u}}_x,\ \tilde{\tilde{u}}_m)$ solves

$$\begin{array}{rcll} -\nabla\cdot D_x(\mathbf{x})\nabla\tilde{\tilde{u}}_x(\mathbf{x}) + \sigma_x\tilde{\tilde{u}}_x(\mathbf{x}) &=& -\delta\sigma_{x,f}\tilde{u}_x, & \text{in } \Omega \\ -\nabla\cdot D_m(\mathbf{x})\nabla\tilde{\tilde{u}}_m(\mathbf{x}) + \sigma_m\tilde{\tilde{u}}_m(\mathbf{x}) &=& \eta(\sigma_{x,f} + \delta\sigma_{x,f})\tilde{\tilde{u}}_x + \eta\delta\sigma_{x,f} v_x, & \text{in } \Omega \\ \tilde{\tilde{u}}_x(\mathbf{x}) = 0, \quad \tilde{\tilde{u}}_m(\mathbf{x}) &=& 0, & \text{on } \partial\Omega. \end{array} \tag{36}$$

We observe, following the same argument in the proof of Lemma 2.1 that (36) admits a unique solution. Moreover, standard stability results in [41, 46, 70, 80] imply that

$$\|(\tilde{\tilde{u}}_x, \tilde{\tilde{u}}_m)\|_{[\mathcal{H}^k(\Omega)]^2} \leq \tilde{c}\|\delta\sigma_{x,f}\|_{L^\infty(\Omega)}\|(\tilde{u}_x, v_x)\|_{[L^2(\Omega)]^2}, \quad k = 0, 1, 2. \tag{37}$$

Also, we observe from the first equation in (33) and the first equation in (35) that

$$\|(\tilde{u}_x, v_x)\|_{[L^2(\Omega)]^2} \leq \tilde{\tilde{c}}\|\delta\sigma_{x,f}\|_{L^\infty(\Omega)}\|u_x\|_{L^2(\Omega)}. \tag{38}$$

We then deduce that

$$\|(\tilde{\tilde{u}}_x, \tilde{\tilde{u}}_m)\|_{[\mathcal{H}^k(\Omega)]^2} \leq c\|\delta\sigma_{x,f}\|^2_{L^\infty(\Omega)}\|u_x\|_{L^2(\Omega)}, , \quad k = 0, 1, 2 \tag{39}$$

which then leads to, for $k = 0, 1, 2$

$$\lim_{\|\delta\sigma_{x,f}\|_{L^\infty(\Omega)}\to 0} \frac{\|(\tilde{\tilde{u}}_x, \tilde{\tilde{u}}_m)\|_{[\mathcal{H}^k(\Omega)]^2}}{\|\delta\sigma_{x,f}\|_{L^\infty(\Omega)}} \equiv \lim_{\|\delta\sigma_{x,f}\|_{L^\infty(\Omega)}\to 0} \frac{\|(u'_x - u_x - v_x, u'_m - u_m - v_m)\|_{[\mathcal{H}^k(\Omega)]^2}}{\|\delta\sigma_{x,f}\|_{L^\infty(\Omega)}} = 0. \tag{40}$$

Standard elliptic theory on maximum principles allows us to replace the $\mathcal{H}^k$ norms and the $L^2(\Omega)$ norms in (37)- (40) with the $L^\infty(\Omega)$ norm. This shows that (u_x, u_m) is Fréchet differentiable with respect to $\sigma_{x,f}$ as a map: $L^\infty(\Omega) \times L^\infty(\Omega) \mapsto \mathcal{H}^k(\Omega) \times \mathcal{H}^k(\Omega)$ $(k = 0, 1, 2)$ (which we will need in Section 4) and as a map: $L^\infty(\Omega) \times L^\infty(\Omega) \mapsto L^\infty(\Omega) \times L^\infty(\Omega)$. This completes the proof. □

To reconstruct both $\delta\eta$ and $\delta\sigma_{x,f}$, a simple dimension counting implies that we have to have at least two data sets. We denote by $(u_{x|j}, u_{m|j})$ $(1 \leq j \leq J$, J being the total number of data sets available) the solution to the background problem with coefficient $\sigma_{x,f}$, under excitation $g_{x|j}$. Then equations for the perturbed quantities take the forms of (33) and (34):

$$\begin{array}{rcll} -\nabla \cdot D_x(\mathbf{x})\nabla v_{x|j}(\mathbf{x}) + \sigma_x v_{x|j}(\mathbf{x}) &=& -\delta\sigma_{x,f}u_{x|j}, & \text{in } \Omega \\ -\nabla \cdot D_m(\mathbf{x})\nabla v_{m|j}(\mathbf{x}) + \sigma_m v_{m|j}(\mathbf{x}) &=& \eta\sigma_{x,f}v_{x|j} + \eta\delta\sigma_{x,f}u_{x|j}, & \text{in } \Omega \\ -\nabla \cdot D_m(\mathbf{x})\nabla w_{m|j}(\mathbf{x}) + \sigma_m w_{m|j}(\mathbf{x}) &=& \delta\eta\sigma_{x,f}u_{x|j}, & \text{in } \Omega \\ v_{x|j}(\mathbf{x}) = 0, \quad v_{m|j}(\mathbf{x}) = 0, \quad w_{m|j} &=& 0, & \text{on } \partial\Omega. \end{array} \tag{41}$$

The perturbed data sets are given as

$$\frac{1}{\Xi}dH_j[\eta, \sigma_{x,f}](\delta\eta, \delta\sigma_{x,f}) = \sigma_m w_{m|j} + \delta\sigma_{x,f}u_{x|j} + \sigma_x v_{x|j} + \sigma_m v_{m|j}, \quad 1 \leq j \leq J. \tag{42}$$

The equations in (41), together with those in (42), form a system of linear equations for $(v_{x|j}, v_{m|j}, w_{m|j})$ $(1 \leq j \leq J)$, $\delta\eta$, and $\delta\sigma_{x,f}$. We now analyze the problem in some simplified settings.

Linearization around (0, 0). Let us first consider the simplified situation where the background coefficients $(\eta, \sigma_{x,f}) = (0, 0)$ and we have one data set. In this setting, the perturbed data (42) simplified to

$$\frac{1}{\Xi}dH[0, 0](\delta\eta, \delta\sigma_{x,f}) = \delta\sigma_{x,f}u_x + \sigma_{x,i}v_x \tag{43}$$

and the equations for the perturbation (41) simplified to

$$-\nabla\cdot D_x(\mathbf{x})\nabla v_x(\mathbf{x})+\sigma_{x,i}v_x(\mathbf{x})=-\delta\sigma_{x,f}u_x,\quad \text{in}\ \ \Omega,\qquad v_x=0,\quad \text{on}\ \ \partial\Omega. \tag{44}$$

We observe immediately that $\delta\eta$ completely disappears from (43) and (44). This means that we would not be able to reconstruct $\delta\eta$ in this setting, no matter how many data sets we have. However, we can uniquely and stably reconstruct $\delta\sigma_{x,f}$ with only one data set ($J=1$) as stated in the following result.

Proposition 3.6. *Let $dH[0,0]$ and $d\tilde{H}[0,0]$ be two perturbed data sets in the form of (43), generated with perturbed coefficients $(\delta\eta,\ \delta\sigma_{x,f})$ and $(\widetilde{\delta\eta},\ \widetilde{\delta\sigma}_{x,f})$ respectively. Then $dH[0,0]=d\tilde{H}[0,0]$ implies $\delta\sigma_{x,f}=\widetilde{\delta\sigma}_{x,f}$. In addition, we have*

$$\|(\delta\sigma_{x,f}-\widetilde{\delta\sigma}_{x,f})u_x\|_{L^2(\Omega)}\leq c\|dH[0,0]-d\tilde{H}[0,0]\|_{L^2(\Omega)} \tag{45}$$

with c a constant that depends on Ω, D_x, $\sigma_{x,i}$ and Ξ.

Proof. We combine (43) and (44) to obtain

$$-\nabla\cdot D_x(\mathbf{x})\nabla v_x(\mathbf{x})=-dH[0,0]/\Xi,\quad \text{in}\ \ \Omega,\qquad v_x=0,\quad \text{on}\ \ \partial\Omega. \tag{46}$$

This equation admits a unique solution $v_x\in\mathcal{H}^2(\Omega)$. The unknown $\delta\sigma_{x,f}$ can then be uniquely reconstructed by inserting v_x in the data (43). The data (43) also leads to

$$\|(\delta\sigma_{x,f}-\widetilde{\delta\sigma}_{x,f})u_x\|_{L^2(\Omega)}\leq\tilde{c}_1\big(\|dH[0,0]-d\tilde{H}[0,0]\|_{L^2(\Omega)}+\|v_x-\tilde{v}_x\|_{L^2(\Omega)}\big), \tag{47}$$

with $\tilde{c}_1$ depending on $\sigma_{x,i}$ and Ξ. The stability result (45) then follows from (47) and the following stability estimate for the PDE (46)

$$\|v_x-\tilde{v}_x\|_{L^2(\Omega)}\leq\tilde{c}_2\|dH[0,0]-d\tilde{H}[0,0]\|_{L^2(\Omega)}, \tag{48}$$

where $\tilde{c}_2$ depends on Ω, D_x and Ξ. □

The above result provides the following reconstruction algorithm for recovering $\delta\sigma_{x,f}$ around the background $(\eta,\sigma_{x,f})=(0,0)$.

Algorithm III (A): To reconstructing $\delta\sigma_{x,f}$.

S1. Given data $dH[0,0]$, solve (46) to recover v_x;

S2. Reconstruct $\delta\sigma_{x,f}$ as $\delta\sigma_{x,f}=(dH[0,0]/\Xi-\sigma_{x,i}v_x)/u_x$.

Linearization around ($\eta\not\equiv 0,\ 0$). We now consider a simplified situation where the background coefficients $\eta\not\equiv 0$, $\sigma_{x,f}=0$. We observe again that $\delta\eta$ disappears from the data (42) and the equations for the perturbations (41). Thus it is not possible to reconstruct the two perturbed coefficients simultaneously. However, the background coefficient η and the perturbation $\delta\sigma_{x,f}$ both appear. We now attempt to reconstruct both of them simultaneously using two data sets.

We denote by $G_{D,\sigma}$ the Green function for the operator $-\nabla\cdot D\nabla+\sigma$ with homogeneous Dirichlet boundary condition. Then we can express the perturbed internal data dH_j as

$$\frac{1}{\Xi}dH_j[\eta,0](\delta\eta,\delta\sigma_{x,f}) \;=\; \sigma_m K_{m|j}(\vartheta)+u_{x|j}\delta\sigma_{x,f}-\sigma_{x,i}K_{x|j}(\delta\sigma_{x,f}),\quad 1\le j\le 2. \tag{49}$$

where $\vartheta=\eta\delta\sigma_{x,f}$, and the operators $K_{m|j}$ and $K_{x|j}$ are respectively defined as,

$$K_{m|j}(\vartheta) \;=\; \int_\Omega G_{D_m,\sigma_m}(\mathbf{y};\mathbf{x})u_{x|j}(\mathbf{y})\vartheta(\mathbf{y})d\mathbf{y}, \tag{50}$$

$$K_{x|j}(\delta\sigma_{x,f}) \;=\; \int_\Omega G_{D_x,\sigma_{x,i}}(\mathbf{y};\mathbf{x})u_{x|j}(\mathbf{y})\delta\sigma_{x,f}(\mathbf{y})d\mathbf{y}. \tag{51}$$

Note that, as in the previous case, $\delta\eta$ completely disappear from (43) and (44). This means that we would not be able to reconstruct $\delta\eta$ in this setting, no matter how many data sets we have.

Since the background solutions $u_{x|j}$ $(1\le j\le 2)$ are bounded, classical elliptic theory [41, 46, 70] then implies that $K_{x|j}$ and $K_{m|j}$ are *compact* linear (and thus bounded) operators from $L^2(\Omega)$ to $\mathcal{H}_0^2(\Omega)$ with the assumptions on the coefficients in (**A-i**). Thanks to the compact emeddie bauerbedding of $\mathcal{H}_0^2(\Omega)$ in $L^2(\Omega)$ [1, 124], the map $\frac{1}{\Xi}dH_j[\eta,0]:L^2(\Omega)\times L^2(\Omega)\mapsto L^2(\Omega)$ is compact. Let us define the matrix operator $K:L^2(\Omega)\times L^2(\Omega)\mapsto L^2(\Omega)\times L^2(\Omega)$

$$K=\begin{pmatrix}\sigma_m K_{m|1} & u_{x|1}\mathcal{I}-\sigma_{x,i}K_{x|1}\\ \sigma_m K_{m|2} & u_{x|2}\mathcal{I}-\sigma_{x,i}K_{x|2}\end{pmatrix} \tag{52}$$

and denote by $\mathcal{N}(K)$ the null space of K, then the following results follows immediately from (49).

Theorem 3.7. *Let $d\mathbf{H}=(dH_1[\eta,0],dH_2[\eta,0])$ and $d\widetilde{\mathbf{H}}=(d\widetilde{H}_1[\eta,0],d\widetilde{H}_2[\eta,0])$ be two perturbed data sets generated with perturbed coefficients $(\vartheta,\,\delta\sigma_{x,f})$ and $(\widetilde{\vartheta},\,\widetilde{\delta\sigma}_{x,f})$ respectively. Then we have*

$$c_1\|d\mathbf{H}-d\widetilde{\mathbf{H}}\|_{(L^2(\Omega))^2}\le\|(\vartheta,\delta\sigma_{x,f})-(\widetilde{\vartheta},\widetilde{\delta\sigma}_{x,f})\|_{(L^2(\Omega))^2/\mathcal{N}(K)}\le c_2\|d\mathbf{H}-d\widetilde{\mathbf{H}}\|_{(L^2(\Omega))^2}. \tag{53}$$

Remark 3.8. We notice that as long as we can choose excitations $g_{x|j}$ such that $u_{x|j}\ge c_0>0$ inside Ω for some c_0, the operators $u_{x|j}\mathcal{I}-\sigma_{x,i}K_{x|j}$ will be invertible, and $\sigma_m K_{m|j}$ are always invertible. To make K invertible, in which case $\mathcal{N}(K)=\{(0,0)\}$ and we have uniqueness of reconstructing $(\vartheta,\delta\sigma_{x,f})$ (and thus $(\eta,\delta\sigma_{x,f})$), we have to be able to select two excitations $g_{x|1}$ and $g_{x|2}$ such that the operator $K_{m|1}^{-1}(\frac{u_{x|1}}{\sigma_m}-\frac{\sigma_{x,i}}{\sigma_m}K_{x|1})-K_{m|2}^{-1}(\frac{u_{x|2}}{\sigma_m}-\frac{\sigma_{x,i}}{\sigma_m}K_{x|1})$ (or equivalently $(u_{x|1}-\sigma_{x,i}K_{x|1})^{-1}K_{m|1}-(u_{x|2}-\sigma_{x,i}K_{x|2})^{-1}K_{m|2}$) is invertible. We do not have a more explicit characterization of this injectivity condition at the moment. Note that the result we have here is based on the availability of two data sets $dH_1[\eta,0]$ and $dH_2[\eta,0]$. When we have access to more data sets, it might be possible to establish the injectivity of the map (42) following, for instance, the techniques in [12, 66]. We leave this issue to future studies.

Remark 3.9. It turns out that the problem linearized around $(0,\sigma_{x,f}\not\equiv 0)$ has exactly the same structure as the case we just analyzed if we define the variable ϑ as $\vartheta=\sigma_{x,f}\delta\eta$.

Linearization around a general background. We now consider the linearization around arbitrary background coefficients ($\eta \not\equiv 0, \sigma_{x,f} \not\equiv 0$) with overdetermined data sets ($J > 2$). Let us introduce two more linear integral operators

$$K^{\eta}_{m|j}(\delta\sigma_{x,f}) = \int_{\Omega} \eta(\mathbf{y}) G_{D_m,\sigma_m}(\mathbf{y};\mathbf{x}) u_{x|j}(\mathbf{y}) \delta\sigma_{x,f}(\mathbf{y}) d\mathbf{y}, \tag{54}$$

$$K_{mx|j}(\delta\sigma_{x,f}) = \int_{\Omega} \eta(\mathbf{y}) \sigma_{x,f}(\mathbf{y}) G_{D_m,\sigma_m}(\mathbf{y};\mathbf{x}) K_{x|j}(\delta\sigma_{x,f})(\mathbf{y}) d\mathbf{y}. \tag{55}$$

Both $K^{\eta}_{m|j}$ and $K_{mx|j}$ are *compact* linear (and thus bounded) operators from $L^2(\Omega)$ to $\mathcal{H}^2_0(\Omega)$ with the assumptions on the coefficients in (**A-i**). We can now express the perturbed perturbed data $dH_j[\eta, \sigma_{x,f}]$ as, $\quad 1 \le j \le J$,

$$\frac{1}{\Xi} dH_j[\eta,\sigma_{x,f}](\delta\eta,\delta\sigma_{x,f}) = \sigma_m K_{m|j}(\vartheta) + u_{x|j}\delta\sigma_{x,f} - \sigma_x K_{x|j}(\delta\sigma_{x,f}) + \sigma_m K^{\eta}_{m|j}(\delta\sigma_{x,f}) - \sigma_m K_{mx|j}(\delta\sigma_{x,f}) \tag{56}$$

where $\vartheta = \sigma_{x,f}\delta\eta$.

We solve this overdetermined system of equations in the regularized (linear) least-square sense. That is, we look for a pair $(\vartheta, \delta\sigma_{x,f})$ that minimizes

$$\sum_{j=1}^{J} \| \frac{dH_j[\eta,\sigma_{x,f}]}{\Xi} - \bar{K}_{m|j}(\vartheta) - \bar{K}_{x|j}(\delta\sigma_{x,f}) \|^2_{L^2(\Omega)} + \beta(\|\nabla\vartheta\|^2_{[L^2(\Omega)]^d} + \|\nabla\delta\sigma_{x,f}\|^2_{[L^2(\Omega)]^d}) \tag{57}$$

where short notations $\bar{K}_{m|j} = \sigma_m K_{m|j}$ and $\bar{K}_{x|j} = u_{x|j}\mathcal{I} - \sigma_x K_{x|j} + \sigma_m K^{\eta}_{m|j} - \sigma_m K_{mx|j}$ are employed, and the regularization term, with strength parameter β, is used to deal with noise in the data. Classical least-square theory then gives the solution as

$$\begin{pmatrix} \vartheta \\ \delta\sigma_{x,f} \end{pmatrix} = \begin{pmatrix} \sum_{j=1}^{J} \bar{K}^*_{m|j}\bar{K}_{m|j} + \beta L & \sum_{j=1}^{J} \bar{K}^*_{m|j}\bar{K}_{x|j} \\ \sum_{j=1}^{J} \bar{K}^*_{x|j}\bar{K}_{m|j} & \sum_{j=1}^{J} \bar{K}^*_{x|j}\bar{K}_{x|j} + \beta L \end{pmatrix}^{-1} \begin{pmatrix} \sum_{j=1}^{J} \bar{K}^*_{m|j}\frac{dH_j}{\Xi} \\ \sum_{j=1}^{J} \bar{K}^*_{x|j}\frac{dH_j}{\Xi} \end{pmatrix} \tag{58}$$

where the operator A^* is the adjoint of A, and the operator L is defined as $L(\phi) = -\Delta\phi + (\mathbf{n}\cdot\nabla\phi)_{|\partial\Omega}$. The following algorithm can be implemented to reconstruct the pair $(\delta\eta, \delta\sigma_{x,f})$.

Algorithms III (B): To reconstruct $(\delta\eta, \delta\sigma_{x,f})$.

S1. Find minimizer of (57) by using a minimization algorithm or formula (58);

S2. Reconstruct $\delta\eta = \vartheta/\sigma_{x,f}$.

Remark 3.10. Note that here it is assumed that the inverse of the (regularized) normal operator in (58) is well-defined. This is clearly not guaranteed with the form of regularization taken here. Numerically we observe that this always the case when excitations $g_{x|j}$, $1 \le j \le J$ are chosen sufficiently different. In fact, with data collected from 4 or more excitations, we never observe the failure of the invertibility, even in the case $\beta = 0$. The theoretical analysis of the issue following the techniques in [12, 66] is undergoing.

4 Reconstruction algorithm

We now present a numerical procedure to reconstruct $(\eta, \sigma_{x,f})$ by solving the full nonlinear inverse problem. The procedure is based on Newton's method for nonlinear least-square problems. We intend to minimize

$$\mathcal{F}[\eta, \sigma_{x,f}] = \frac{1}{2}\sum_{j=1}^{J} \|H_j[\eta, \sigma_{x,f}] - H_j^*\|^2_{L^2(\Omega)} + \frac{\beta}{2}(\|\nabla\eta\|^2_{[L^2(\Omega)]^d} + \|\nabla\sigma_{x,f}\|^2_{[L^2(\Omega)]^d}) \tag{59}$$

where $H_j[\eta, \sigma_{x,f}]$ is the functional defined in (6) for $g_{x|j}$ while H_j^* is the corresponding interior data obtained from acoustic inversion.

We solve the minimization problem with the Newton's method which minimizes the functional (59) through an iterative process. Suppose we know the parameters at iteration $\ell \geq 0$, $(\eta^\ell,\, \sigma^\ell_{x,f})$, Newton's method update the parameters by

$$(\eta^{\ell+1}, \sigma^{\ell+1}_{x,f}) = (\eta^\ell, \sigma^\ell_{x,f}) + \alpha^\ell(\delta\eta^\ell, \delta\sigma^\ell_{x,f}) \tag{60}$$

where $(\delta\eta^\ell, \delta\sigma^\ell_{x,f})$ is the direction of the update, and α^ℓ is the step length in that direction. The direction of the update is obtained by solving the following system, often known as the Karush-Kuhn-Tucker (KKT) condition [86]:

$$\begin{aligned} d_1(d_1\mathcal{F}[\eta^\ell, \sigma^\ell_{x,f}](\hat\eta))(\delta\eta^\ell) + d_2(d_1\mathcal{F}[\eta^\ell, \sigma^\ell_{x,f}](\hat\eta))(\delta\sigma^\ell_{x,f}) &= -d_1\mathcal{F}[\eta^\ell, \sigma^\ell_{x,f}](\hat\eta) \\ d_1(d_2\mathcal{F}[\eta^\ell, \sigma^\ell_{x,f}](\hat\sigma_{x,f}))(\delta\eta^\ell) + d_2(d_2\mathcal{F}[\eta^\ell, \sigma^\ell_{x,f}](\hat\sigma_{x,f}))(\delta\sigma^\ell_{x,f}) &= -d_2\mathcal{F}[\eta^\ell, \sigma^\ell_{x,f}](\hat\sigma_{x,f}) \end{aligned} \tag{61}$$

with $(\hat\eta,\, \hat\sigma_{x,f})$ a pair of test functions. Using the same argument as in Lemma 3.5, it can be shown that the map $H : (\eta, \sigma_{x,f}) \mapsto H = \Xi(\sigma u_x + \sigma_m u_m)$ has second order Fréchet derivatives, which then, together with the chain rule, implies that $\mathcal{F}$ has the second order Fréchet derivatives needed in (61). These derivatives are presented in the Appendix without giving detailed calculations. In the numerical implementation, we calculate the derivatives directly from the discretized version of the objective functional and the systems of PDEs involved.

The step length α^ℓ is obtained through a simple bisection line search process that ensure the Wolfe conditions [86, 98]. That is, we look for an α^ℓ that solves:

$$\min_{\alpha^\ell > 0} \mathcal{F}[\eta^\ell + \alpha^\ell\delta\eta^\ell, \sigma^\ell_{x,f} + \alpha^\ell\delta\sigma^\ell_{x,f}], \tag{62}$$

and satisfies:

$$\begin{aligned} \mathcal{F}[\eta^{\ell+1}, \sigma^{\ell+1}_{x,f}] &\leq \mathcal{F}[\eta^\ell, \sigma^\ell_{x,f}] + c_1\alpha^\ell\big[d_1\mathcal{F}[\eta^\ell, \sigma^\ell_{x,f}](\delta\eta^\ell) + d_2\mathcal{F}[\eta^\ell, \sigma^\ell_{x,f}](\delta\sigma^\ell_{x,f})\big] \\ d_1\mathcal{F}[\eta^{\ell+1}, \sigma^{\ell+1}_{x,f}](\delta\eta^\ell) + d_2\mathcal{F}[\eta^{\ell+1}, \sigma^{\ell+1}_{x,f}](\delta\sigma^\ell_{x,f}) &\geq c_2\big[d_1\mathcal{F}[\eta^\ell, \sigma^\ell_{x,f}](\delta\eta^\ell) + d_2\mathcal{F}[\eta^\ell, \sigma^\ell_{x,f}](\delta\sigma^\ell_{x,f})\big] \end{aligned}$$

with the constants $c_1 = 10^{-4}$ and $c_2 = 0.1$.

We now have the following Newton's method.

Algorithms IV: To reconstruct $(\eta,\, \sigma_{x,f})$.

S1. Set $\ell = 0$ and the initial guess $(\eta^0,\, \sigma^0_{x,f})$;

S2. Solve sequentially the equations (11), (65) and (66) for $1 \leq j \leq J$, and form the first-order derivatives (67) and (68);

S3. Solve the equations (69), (70), (71), (73), (75) and (77) for $1 \leq j \leq J$, and form the second-order derivatives (72), (74), (76) and (78).

S4. Solve the system (61) for $(\delta\eta^\ell, \delta\sigma_{x,f}^\ell)$, and form ;

S5. Perform the line search to determine α^ℓ;

S6. Update the coefficients according to (60);

S7. If stopping criteria satisfied, stop; otherwise, set $\ell = \ell + 1$ and go to S2.

5 Numerical experiments

We now present some numerical simulations based on synthetic data to validate the results we obtained in the previous section. For the simplicity of simulations, we restrict ourselves to two-dimensional settings even though the theoretical results are independent of dimension. All the PDEs involved are discretized with a first-order finite element method on triangular meshes. The domain of the reconstruction is the square $\Omega = (0,1) \times (0,1)$. The background coefficients are taken as

$$D_x(\mathbf{x}) = D_m(\mathbf{x}) = 0.03 + 0.01 \sin(\pi y), \qquad \sigma_{x,i}(\mathbf{x}) = \sigma_m(\mathbf{x}) = 0.3 + 0.1 \sin(\pi x) \sin(\pi y). \quad (63)$$

To check the impact of the background coefficients on the reconstructions, we performed the same type of reconstructions on different backgrounds. We did *not* observe any substantial difference between reconstructions at different backgrounds. Thus in the rest of the section we only present results that are obtained with the background coefficients given in (63).

The synthetic data are generated by solving the diffusion problem (11) for *known* quantum efficiency η and absorption coefficient $\sigma_{x,f}$. To reduce the degree of "inverse crimes", we use two different sets of finite element meshes when generating the synthetic data and when performing the numerical reconstructions. In general, the meshes for generating data are roughly twice as fine as the meshes used in the inversion, in terms of the numbers of nodes in the meshes. The results we show below are interpolated on uniform grids using the MATLAB interpolation function `griddata`. We performed reconstructions using both noiseless and noisy synthetic data. For the noisy data, we added additive random noise to the data by simply multiplying each datum by $(1 + \gamma \times 10^{-2}$ `random`$)$ with `random` a uniformly distributed random variable taking values in $[-1,\ 1]$, γ being the noise level in percentage. In each case below, we perform reconstructions using three types of data:

- Type (i): noiseless data ($\gamma = 0$);
- Type (ii): data containing 2% random noise ($\gamma = 2$);
- Type (iii): data containing 8% random noise ($\gamma = 8$).

We emphasize that *data in (i) still contain noise that come from interpolating from the forward meshes to the inversion meshes.* We use the relative L^2 error to measure the quality of the reconstructions. This error is defined as the L^2 norm of the difference between the reconstructed coefficient and the true coefficient, divided by the L^2 norm of the true coefficient and then multiplied by 100.

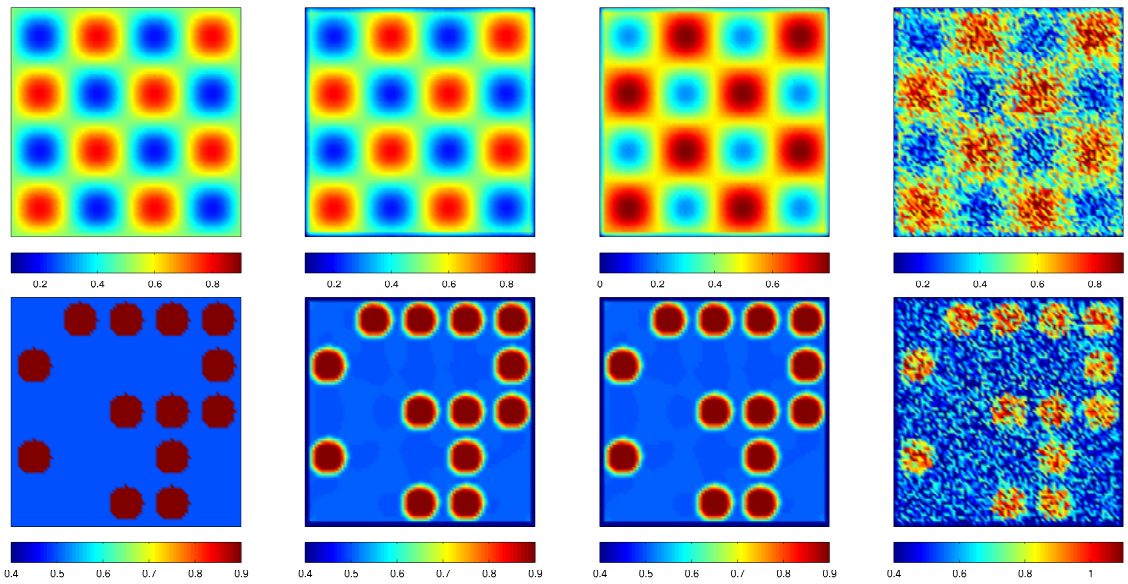

Figure 1: Reconstructions of a smooth (top row) and a piecewise constant (bottom row) quantum efficiency. Shown from left to right are: true η, reconstructions with data (i), reconstructions with data (ii), and reconstructions with data (iii).

Experiment 1. In the first set of numerical experiments, we study the reconstruction of the quantum efficiency η assuming that $\sigma_{x,f}$ is known. The reconstructions are done with Algorithm I. We show in the top row of Fig. 1 the reconstructions of a smooth η. Shown, from left to right, are true η, reconstruction with noiseless data (i), reconstruction with noisy data (ii), and reconstruction with noisy data (iii). The relative L^2 error in the reconstructions are 0.84%, 1.82%, and 6.23% for reconstructions with data types (i), ii) and (iii) respectively. On the bottom row of Fig. 1, we show the same reconstructions for a piecewise constant η. The quality of the reconstructions is similar to that in the smooth coefficient case. The relative L^2 error are 1.11%, 1.98%, 6.87%, respectively. In all those reconstructions, we have preprocessed the data by a 5-point averaging filtering process. Otherwise, the noise in the data are amplified too much by the differentiation operation in the reconstruction algorithm. We did not try more advanced de-noising techniques, but that is an important aspect that deserves further investigation.

Experiment 2. In the second set of numerical experiments, we consider the reconstruction of the fluorescence absorption coefficient $\sigma_{x,f}$ assuming that η is known. We show in Fig. 2 the reconstructions of two different $\sigma_{x,f}$. The reconstructions are done with Algorithm II. Shown, from left to right, are the true η and reconstructions with data of type (i), (ii) and (iii) respectively. The relative L^2 error for reconstructions in the top row are 0.74%, 1.68%, and 5.46% respectively, and those for the reconstructions in the bottom row are 0.82%, 1.57%, and 5.24% respectively. Even though this inverse problem is nonlinear, each reconstruction costs only one forward solution of the elliptic system (20). Thus the reconstructions are very fast. Note that, unlike in Experiment 1, no pre-smoothing of the data is needed in this case.

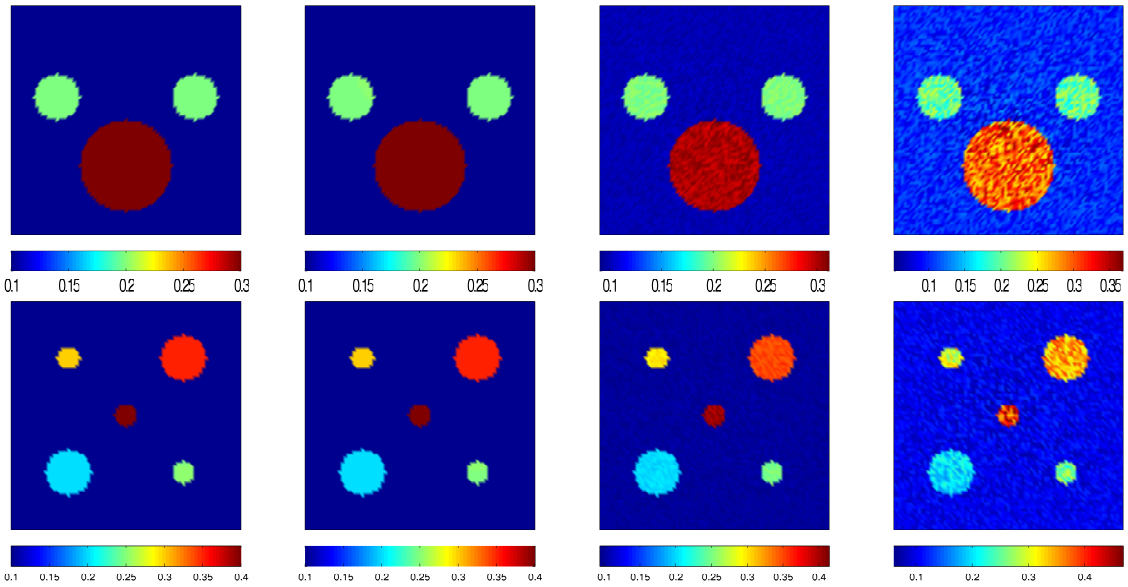

Figure 2: Reconstruction of two different fluorescence absorption coefficients. Shown from left to right are the true $\sigma_{x,f}$, and the reconstructions with data (i), (ii) and (iii) respectively.

Experiment 3. We now attempt to reconstruct the two coefficients η and $\sigma_{x,f}$ simultaneously. We first consider reconstructions in the linearized setting using Algorithm III. The background coefficients are $(\eta^0, \sigma^0_{x,f}) = (0.1, 0.0)$. In Fig. 3 we show reconstructions of perturbed coefficients that are very large. In this specific setting, we completely neglect the error in the data that are caused by linearization. This is done by generating the perturbed data using directly the linearized model (42), *not the nonlinear model* (6). Our aim here is to test the stability of the reconstruction, not the accuracy of the linearization. The reconstructions are done with two data sets that are constructed from excitations

$$g_{x|1}(\mathbf{x}) = \begin{cases} 1, & \mathbf{x} \in \partial\Omega_L \cup \partial\Omega_B \\ 2, & \mathbf{x} \in \partial\Omega_R \cup \partial\Omega_T \end{cases} \quad \text{and} \quad g_{x|2}(\mathbf{x}) = \begin{cases} 1, & \mathbf{x} \in \partial\Omega_R \\ 2, & \mathbf{x} \in \partial\Omega_T \\ 4, & \mathbf{x} \in \partial\Omega_L \cup \partial\Omega_B \end{cases} \tag{64}$$

where $\partial\Omega_L$, $\partial\Omega_B$, $\partial\Omega_R$, and $\partial\Omega_T$ are the left, bottom, right, and top sides of the boundary respectively. The relative L^2 error in the three reconstructions are (1.34%, 1.47%), (1.66%, 1.82), and (7.12%, 6.77%) respectively.

Experiment 4. In the last set of numerical experiments, we show reconstructions of the two coefficients using nonlinear minimization algorithm described in Algorithm IV. In Fig. 4 we show results reconstructed using data with different noise-levels using four data sets. We observe that the algorithm converges from almost all initial guesses we tested, many very far from the true coefficients. In the results shown in Fig. 4, the regularization parameter is taken as $\beta = 10^{-7}, 10^{-5}, 10^{-4}$ respectively in the three reconstructions. These values are obtained by a few trials. Larger β results in smoother reconstructions. However, we did not tune this parameter systematically to obtain the best results. The relative L^2 error in the three reconstructions are (1.41%, 1.22%), (1.86%, 1.79), and (8.01%, 6.94%) respectively.

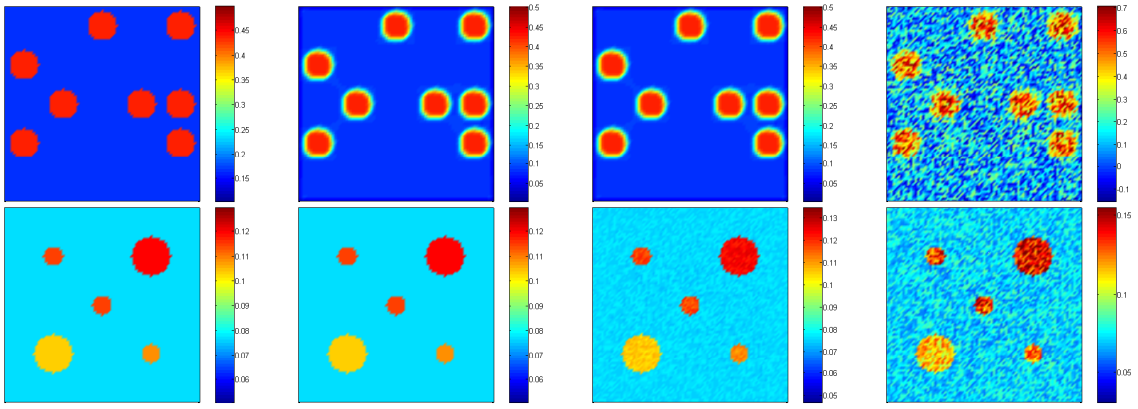

Figure 3: Reconstruction of η (top, superposed on η^0) and $\delta\sigma_{x,f}$ (bottom, superposed on $\sigma^0_{x,f}$). Shown from left to right are the true coefficient, and the reconstructions with data type (i), (ii) and (iii) respectively. Synthetic data used in these reconstructions are generated from the linearized model (42).

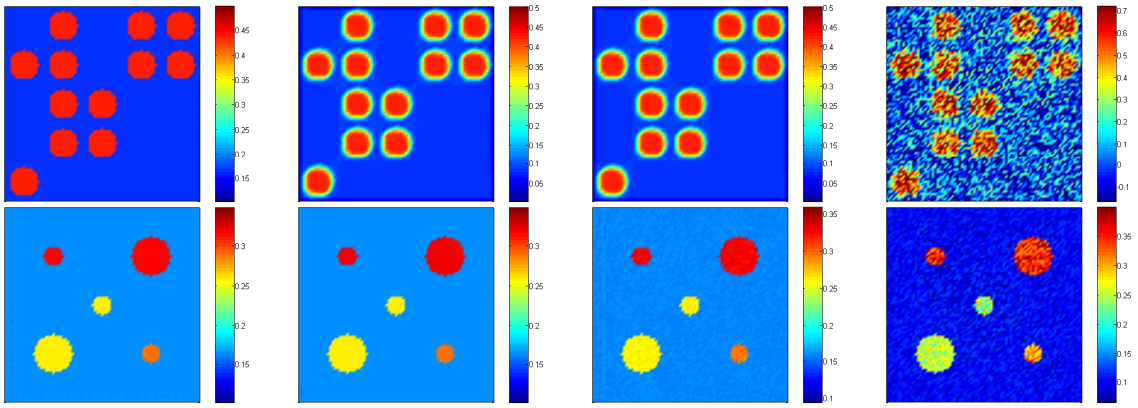

Figure 4: Simultaneous reconstruction of η (top) and $\sigma_{x,f}$ (bottom) with the Newton's method implemented in Algorithm IV. Shown from left to right are the true coefficient, the reconstructions with data of type (i), (ii) and (iii) respectively.

6 Concluding remarks

We proposed in this work a hybrid imaging modality, fluorescence photoacoustic tomography (fPAT), that combines classical ultrasound imaging with fluorescence optical tomography to improve the resolution of the classical fluorescence optical tomography. We presented a set of mathematical models for this hybrid imaging modality which can be viewed as a variant of the usual photoacoustic tomography (PAT) modality.

We studied some inverse problems in the second step of fPAT. We showed that one can uniquely and stably reconstruct either the quantum efficiency η or the fluorescence absorption coefficient $\sigma_{x,f}$ with one interior data obtained from acoustic inversion in the first step of fPAT. In the linearized setting, we showed that one can reconstruct simultaneously the coefficient $\sigma_{x,f}$ and the coefficient η when two "well-selected" data sets are available. Numerical simulations with synthetic data confirm these theoretical results.

There are still many open questions to be addressed. For instance, in the linearized problem of reconstructing $(\delta\eta,\delta\sigma_{x,f})$, we have to assume that there are two excitation patterns that can generate $u_{x|1}$ and $u_{x|2}$ such that the operator $K_{m|1}^{-1}(\frac{u_{x|1}}{\sigma_m} - \frac{\sigma_{x,i}}{\sigma_m}K_{x|1}) - K_{m|2}^{-1}(\frac{u_{x|2}}{\sigma_m} - \frac{\sigma_{x,i}}{\sigma_m}K_{x|1})$ mentioned in Theorem 3.7 is invertible. This will guarantee the injectivity of the map (42). It might be possible to establish prove rigorously the injectivity (42) with redundant data (i.e. $J > 2$ large) following the ellipticity theory presented in [12, 66] and using the techniques of complex geometric optics solutions to construct the corresponding illumination patterns as in [17, 18]. Meanwhile, redundant data might also be used to improve the stability result in Proposition 3.1 so that differentiation of data can be (partially) avoided in the inversion process. On the nonlinear inverse problem of simultaneous reconstruction of η and $\sigma_{x,f}$, even though the numerical simulations in Section 5 suggest that we can perform stable reconstructions, we do not have a mathematical theory for this case yet. We plan to investigate on these issues in a future work.

Acknowledgment

The work of KR is partially supported by National Science Foundation (NSF) through grant DMS-0914825. HZ is partially supported by NSF grant DMS-1115698 and ONR grant N00014-11-1-0602.

Appendix: Fréchet Derivatives of $\mathcal{F}[\eta, \sigma_{x,f}]$

We collect here the results on the computation of first- and second-order Fréchet derivatives of the objective functional (59) without going through detailed calculations.

To compute the first-order derivatives, let us introduce the adjoint variables $(v_{x|j}, v_{m|j})$ that solve the following system of equation:

$$\begin{aligned} -\nabla\cdot D_x\nabla v_{x|j} + \sigma_x v_{x|j} &= \eta\sigma_{x,f}v_{m|j} + (H_j - H_j^*)\Xi\sigma_x, \quad \text{in } \Omega \\ -\nabla\cdot D_m\nabla v_{m|j} + \sigma_m v_{m|j} &= (H_j - H_j^*)\Xi\sigma_m, \quad \text{in } \Omega \\ v_{x|j} = 0, \quad v_{m|j} &= 0, \quad \text{on } \partial\Omega \end{aligned} \tag{65}$$

and the adjoint variable $w_{m|j}$ that solves the following equation:

$$-\nabla\cdot D_m\nabla w_{m|j} + \sigma_m w_{m|j} = (H_j - H_j^*)\Xi\sigma_m, \quad \text{in } \Omega, \qquad w_{m|j} = 0, \quad \text{on } \partial\Omega. \tag{66}$$

We then compute the first-order derivative $d_1\mathcal{F}[\eta, \sigma_{x,f}](\hat{\eta})$ as:

$$d_1\mathcal{F}[\eta, \sigma_{x,f}](\hat{\eta}) = \langle\sum_{j=1}^{J}\sigma_{x,f}u_{x|j}w_{m|j} - \beta\Delta\eta, \hat{\eta}\rangle_{L^2(\Omega)} + \beta\langle\mathbf{n}\cdot\nabla\eta, \hat{\eta}\rangle_{L^2(\partial\Omega)}, \tag{67}$$

and the first-order derivative $d_2\mathcal{F}[\eta, \sigma_{x,f}](\hat{\sigma}_{x,f})$ as:

$$\begin{aligned} d_2\mathcal{F}[\eta, \sigma_{x,f}](\hat{\sigma}_{x,f}) = \langle\sum_{j=1}^{J}u_{x|j}\big(\eta v_{m|j} - v_{x|j} + (H_j - H_j^*)\Xi\big) - \beta\Delta\sigma_{x,f}, \hat{\sigma}_{x,f}\rangle_{L^2(\Omega)} \\ + \beta\langle\mathbf{n}\cdot\nabla\sigma_{x,f}, \hat{\sigma}_{x,f}\rangle_{L^2(\partial\Omega)}. \end{aligned} \tag{68}$$

Let us further introduce the variables $(\bar{v}_{x,j}, \bar{v}_{m|j})$ as the solution to the system:

$$\begin{array}{rcll} -\nabla \cdot D_x \nabla \bar{v}_{x|j} + \sigma_x \bar{v}_{x|j} & = & -\widetilde{\sigma}_{x,f} u_{x|j}, & \text{in } \Omega \\ -\nabla \cdot D_m \nabla \bar{v}_{m|j} + \sigma_m \bar{v}_{m|j} & = & \eta \sigma_{x,f} \bar{v}_{x|j} + \widetilde{\sigma}_{x,f} \eta u_{x|j}, & \text{in } \Omega \\ \bar{v}_{x|j} = 0, \quad \bar{v}_{m|j} & = & 0, & \text{on } \partial\Omega \end{array} \tag{69}$$

and the variable $\bar{w}_{m|j}$ as the solution to the equation:

$$-\nabla \cdot D_m \nabla \bar{w}_{m|j} + \sigma_m \bar{w}_{m|j} = \widetilde{\eta} \sigma_{x,f} u_{x|j}, \text{ in } \Omega, \qquad \bar{w}_{m|j} = 0, \text{ on } \partial\Omega. \tag{70}$$

To compute $d_1(d_1\mathcal{F}[\eta, \sigma_{x,f}](\hat{\eta}))(\widetilde{\eta})$, we define $\phi_{m|j}$ as the solution of the adjoint equation:

$$-\nabla \cdot D_m \nabla \phi_{m|j} + \sigma_m \phi_{m|j} = (\Xi \sigma_m)^2 \bar{w}_{m|j}, \text{ in } \Omega, \qquad \phi_{m|j} = 0, \text{ on } \partial\Omega \tag{71}$$

We can then compute the derivative as

$$d_1(d_1\mathcal{F}[\eta, \sigma_{x,f}](\hat{\eta}))(\widetilde{\eta}) = \langle \sum_{j=1}^{J} \sigma_{x,f} u_{x|j} \phi_{m|j} - \beta \Delta \widetilde{\eta}, \hat{\eta} \rangle_{L^2(\Omega)} + \langle \mathbf{n} \cdot \nabla \widetilde{\eta}, \hat{\eta} \rangle_{L^2(\partial\Omega)}. \tag{72}$$

To compute $d_2(d_1\mathcal{F}[\eta, \sigma_{x,f}](\hat{\eta}))(\widetilde{\sigma}_{x,f})$, we introduce $\varphi_{x|j}$ as the solution to the adjoint equation:

$$-\nabla \cdot D_m \nabla \varphi_{m|j} + \sigma_m \varphi_{m|j} = X_j \Xi \sigma_m, \text{ in } \Omega, \qquad \varphi_{m|j} = 0, \text{ on } \partial\Omega \tag{73}$$

where $X_j = \Xi(\widetilde{\sigma}_{x,f} u_{x|j} + \sigma_x \bar{v}_{x|j} + \sigma_m \bar{v}_{m|j})$. We can then show that

$$d_2(d_1\mathcal{F}[\eta, \sigma_{x,f}](\hat{\eta}))(\widetilde{\sigma}_{x,f}) = \langle \sum_{j=1}^{J} \sigma_{x,f} \bar{v}_{x|j} w_{m|j} + \widetilde{\sigma}_{x,f} u_{x|j} w_{m|j} + \sigma_{x,f} u_{x|j} \varphi_{m|j}, \hat{\eta} \rangle_{L^2(\Omega)}. \tag{74}$$

To compute $d_1(d_2\mathcal{F}[\eta, \sigma_{x,f}](\hat{\sigma}_{x,f}))(\widetilde{\eta})$, we introduce the variables $(\bar{\varphi}_{x|j}, \bar{\varphi}_{m|j})$ as the solution of system:

$$\begin{array}{rcll} -\nabla \cdot D_x \nabla \bar{\varphi}_{x|j} + \sigma_x \bar{\varphi}_{x|j} & = & \eta \sigma_{x,f} \bar{\varphi}_{m|j} + \widetilde{\eta} \sigma_{x,f} w_{m|j} + \Xi \sigma_m \bar{w}_{m|j} \Xi \sigma_x, & \text{in } \Omega \\ -\nabla \cdot D_m \nabla \bar{\varphi}_{m|j} + \sigma_m \bar{\varphi}_{m|j} & = & (\Xi \sigma_m)^2 \bar{w}_{m|j}, & \text{in } \Omega \\ \bar{\varphi}_{x|j} = 0, \quad \bar{\varphi}_{m|j} & = & 0, & \text{on } \partial\Omega \end{array} \tag{75}$$

We then verify that

$$d_1(d_2\mathcal{F}[\eta, \sigma_{x,f}](\hat{\sigma}_{x,f}))(\widetilde{\eta}) = \langle \sum_{j=1}^{J} u_{x|j} \big[\widetilde{\eta} w_{m|j} + \Xi \sigma_m \bar{w}_{m|j} \Xi - \bar{\varphi}_{x|j} + \eta \bar{\varphi}_{m|j} \big], \hat{\sigma}_{x,f} \rangle_{L^2(\Omega)}. \tag{76}$$

To compute $d_2(d_2\mathcal{F}[\eta, \sigma_{x,f}](\hat{\sigma}_{x,f}))(\widetilde{\sigma}_{x,f})$, we introduce $(\bar{\phi}_{x|j}, \bar{\phi}_{m|j})$ as the solution to the system:

$$\begin{array}{rcll} -\nabla \cdot D_x \nabla \bar{\phi}_{x|j} + \sigma_x \bar{\phi}_{x|j} & = & \eta \sigma_{x,f} \bar{\phi}_{m|j} + Y_j + X_j \Xi \sigma_x, & \text{in } \Omega \\ -\nabla \cdot D_m \nabla \bar{\phi}_{m|j} + \sigma_m \bar{\phi}_{m|j} & = & X_j \Xi \sigma_m, & \text{in } \Omega \\ \bar{\phi}_{x|j} = 0, \quad \bar{\phi}_{m|j} & = & 0, & \text{on } \partial\Omega \end{array} \tag{77}$$

where $Y_j = \widetilde{\sigma}_{x,f}\big((H_j - H_j^*)\Xi - v_{x|j} + \eta v_{m|j}\big)$. We can then compute the derivative as

$$\begin{aligned} d_2(d_2\mathcal{F}[\eta, \sigma_{x,f}](\hat{\sigma}_{x,f}))(\widetilde{\sigma}_{x,f}) = -\beta \langle \Delta \widetilde{\sigma}_{x,f}, \hat{\sigma}_{x,f} \rangle_{L^2(\Omega)} + \beta \langle \mathbf{n} \cdot \nabla \widetilde{\sigma}_{x,f}, \hat{\sigma}_{x,f} \rangle_{L^2(\partial\Omega)} + \\ \langle \sum_{j=1}^{J} (H_j - H_j^*) \Xi \bar{v}_{x|j} - \bar{v}_{x|j} v_{x|j} + \eta \bar{v}_{x|j} v_{m|j} + X_j \Xi u_{x|j} + \big(\eta \bar{\phi}_{m|j} - \bar{\phi}_{x|j}\big) u_{x|j}, \hat{\sigma}_{x,f} \rangle_{L^2(\Omega)}. \end{aligned} \tag{78}$$

References

[1] R. A. Adams, *Sobolev Spaces*, Academic Press, New York, 1975.

[2] M. Agranovsky, P. Kuchment, and E. T. Quinto, *Range descriptions for the spherical mean Radon transform*, J. Funct. Anal., 248 (2007), pp. 344–386.

[3] D. Álvarez, P. Medina, and M. Moscoso, *Fluorescence lifetime imaging from time resolved measurements using a shape-based approach*, Optics Express, 17 (2009), pp. 8843–8855.

[4] G. Ambartsoumian, R. Gouia-Zarrad, and M. Lewis, *Inversion of the circular Radon transform on an annulus*, Inverse Problems, 26 (2010). 105015.

[5] H. Ammari, *An Introduction to Mathematics of Emerging Biomedical Imaging*, Springer, 2008.

[6] H. Ammari, E. Bossy, V. Jugnon, and H. Kang, *Mathematical modelling in photo-acoustic imaging of small absorbers*, SIAM Rev., 52 (2010), pp. 677–695.

[7] ——, *Reconstruction of the optical absorption coefficient of a small absorber from the absorbed energy density*, SIAM J. Appl. Math., 71 (2011), pp. 676–693.

[8] H. Ammari, E. Bretin, J. Garnier, and A. Wahab, *Time reversal in attenuating acoustic media*, Contemporary Mathematics, 548 (2011), pp. 151–163.

[9] H. Ammari, E. Bretin, V. Jugnon, and A. Wahab, *Photo-acoustic imaging for attenuating acoustic media*, Lecture Notes in Mathematics, 2035 (2011), pp. 53–80.

[10] H. Ammari, J. Garnier, and L. Giovangigli, *Mathematical modeling of fluorescence diffuse optical imaging of cell membrane potential changes*, Quarterly of Applied Mathematics, (2012).

[11] G. Bal, *Hybrid inverse problems and internal information*, in Inside Out: Inverse Problems and Applications, G. Uhlmann, ed., Mathematical Sciences Research Institute Publications, Cambridge University Press, 2012.

[12] ——, *Hybrid inverse problems and redundant systems of partial differential equations*, arXiv, 1210.0265 (2012).

[13] G. Bal, A. Jollivet, and V. Jugnon, *Inverse transport theory of photoacoustics*, Inverse Problems, 26 (2010). 025011.

[14] G. Bal and K. Ren, *Multi-source quantitative PAT in diffusive regime*, Inverse Problems, 27 (2011). 075003.

[15] ——, *Non-uniqueness results for a hybrid inverse problem*, in Tomography and Inverse Transport Theory, G. Bal, D. Finch, P. Kuchment, J. Schotland, P. Stefanov, and G. Uhlmann, eds., vol. 559 of Contemporary Mathematics, Amer. Math. Soc., Providence, RI, 2011, pp. 29–38.

[16] ——, *On multi-spectral quantitative photoacoustic tomography in diffusive regime*, Inverse Problems, 28 (2012). 025010.

[17] G. Bal, K. Ren, G. Uhlmann, and T. Zhou, *Quantitative thermo-acoustics and related problems*, Inverse Problems, 27 (2011). 055007.

[18] G. Bal and G. Uhlmann, *Inverse diffusion theory of photoacoustics*, Inverse Problems, 26 (2010). 085010.

[19] ——, *Reconstruction of coefficients in scalar second-order elliptic equations from knowledge of their solutions*, Commun. Pure Appl. Math., (2013).

[20] P. Beard, *Biomedical photoacoustic imaging*, Interface Focus, 1 (2011), pp. 602–631.

[21] P. Burgholzer, H. Grun, and A. Sonnleitner, *Photoacoustic tomography: Sounding out fluorescent proteins*, Nat. Photon., 3 (2009), p. 378379.

[22] P. Burgholzer, G. J. Matt, M. Haltmeier, and G. Paltauf, *Exact and approximative imaging methods for photoacoustic tomography using an arbitrary detection surface*, Phys. Rev. E, 75 (2007). 046706.

[23] J. Chang, R. L. Barbour, and H. Graber, *Imaging of fluorescence in highly scattering media*, IEEE Trans. Biomed. Eng., 44(9) (1997), pp. 810–822.

[24] A. J. Chaudhari, S. Ahn, R. Levenson, R. D. Badawi, S. R. Cherry, and R. M. Leahy, *Excitation spectroscopy in multispectral optical fluorescence tomography: methodology, feasibility and computer simulation studies*, Phys. Med. Biol., 54 (2009), pp. 4687–4704.

[25] J. Chen, V. Venugopal, and X. Intes, *Monte carlo based method for fluorescence tomographic imaging with lifetime multiplexing using time gates*, Biomedical Optics Express, 2 (2011), pp. 871–886.

[26] Y.-Z. Chen and L.-C. Wu, *Second Order Elliptic Equations and Elliptic Systems*, American Mathematical Society, Providence, 2004.

[27] S. R. Cherry, *In vivo molecular imaging and genomic imaging: new challenges for imaging physics*, Phys. Med. Biol., 49 (2004), pp. R13–R48.

[28] A. X. Cong and G. Wang, *Multispectral bioluminescence tomography: Methodology and simulation*, Int. J. Biomed. Imag., 2006 (2006). 57614.

[29] A. Corlu, R. Choe, T. Durduran, M. A. Rosen, M. Schweiger, S. R. Arridge, M. D. Schnall, and A. G. Yodh, *Three-dimensional in vivo fluorescence diffuse optical tomography of breast cancer in humans*, Optics Express, 15 (2007), pp. 6696–6716.

[30] B. T. Cox, S. R. Arridge, and P. C. Beard, *Estimating chromophore distributions from multiwavelength photoacoustic images*, J. Opt. Soc. Am. A, 26 (2009), pp. 443–455.

[31] B. T. Cox, S. R. Arridge, K. P. Köstli, and P. C. Beard, *Two-dimensional quantitative photoacoustic image reconstruction of absorption distributions in scattering media by use of a simple iterative method*, Applied Optics, 45 (2006), pp. 1866–1875.

[32] B. T. Cox and P. C. Beard, *Photoacoustic tomography with a single detector in a reverberant cavity*, J. Opt. Soc. Am. A, 125 (2009), pp. 1426–1436.

[33] B. T. Cox, J. G. Laufer, and P. C. Beard, *The challenges for quantitative photoacoustic imaging*, Proc. of SPIE, 7177 (2009). 717713.

[34] N. Deliolanis, T. Lasser, D. Hyde, A. Soubret, J. Ripoll, and V. Ntziachristos, *Free-space fluorescence molecular tomography utilizing 360 geometry projections*, Opt. Lett., 32 (2007), pp. 382–384.

[35] N. Ducros, A. Bassi, G. Valentini, M. Schweiger, S. Arridge, and C. DAndrea, *Multiple-view fluorescence optical tomography reconstruction using compression of experimental data*, Opt. Lett., 36 (2011), pp. 1377–1379.

[36] N. Ducros, C. DAndrea, A. Bassi, G. Valentini, and S. Arridge, *A virtual source pattern method for fluorescence tomography with structured light*, Phys. Med. Biol., 57 (2012), p. 38113832.

[37] J. Dutta, S. Ahn, A. A. Joshi, and R. M. Leahy, *Illumination pattern optimization for fluorescence tomography: theory and simulation studies*, Phys. Med. Biol., 55 (2010), pp. 2961–2982.

[38] J. Dutta, S. Ahn, C. Li, S. R. Cherry, and R. M. Leahy, *Joint L1 and total variation regularization for fluorescence molecular tomography*, Phys. Med. Biol., 57 (2012), pp. 1459–1476.

[39] P. Elbau, O. Scherzer, and R. Schulze, *Reconstruction formulas for photoacoustic sectional imaging*, arXiv:1109.0841v1, (2011).

[40] M. J. Eppstein, D. J. Hawrysz, A. Godavarty, and E. M. Sevick-Muraca, *Three-dimensional, Bayesian image reconstruction from sparse and noisy data sets: Near-infrared fluorescence tomography*, Proc. Natl. Acad. Sci. USA, 99 (2002), pp. 9619–9624.

[41] L. C. Evans, *Partial Differential Equations*, American Mathematical Society, Providence, RI, 1998.

[42] A. R. Fisher, A. J. Schissler, and J. C. Schotland, *Photoacoustic effect for multiply scattered light*, Phys. Rev. E, 76 (2007). 036604.

[43] H. Gao, Y. Lin, G. Gulsen, and H. Zhao, *Fully linear reconstruction method for fluorescence yield and lifetime through inverse complex-source formulation*, Opt. Lett., 35 (2010), pp. 1899–1901.

[44] H. Gao, S. Osher, and H. Zhao, *Quantitative photoacoustic tomography*, in Mathematical Modeling in Biomedical Imaging II: Optical, Ultrasound, and Opto-Acoustic Tomographies, H. Ammari, ed., Lecture Notes in Mathematics, Springer, 2012.

[45] H. Gao, H. Zhao, and S. Osher, *Bregman methods in quantitative photoacoustic tomography*. CAM Report 10-42, UCLA, 2010.

[46] D. Gilbarg and N. S. Trudinger, *Elliptic Partial Differential Equations of Second Order*, Springer-Verlag, Berlin, 2000.

[47] A. Godavartya, E. M. Sevick-Muraca, and M. J. Eppstein, *Three-dimensional fluorescence lifetime tomography*, Med. Phys., 32 (2005), pp. 992–1000.

[48] E. E. Graves, R. Weissleder, and V. Ntziachristos, *Fluorescence molecular imaging of small animal tumor models*, Current Molecular Medicine, 4 (2004), pp. 419–430.

[49] M. Gurfinkel, S. Ke, X. X. Wen, C. Li, and E. M. Sevick-Muraca, *Near-infrared fluorescence optical imaging and tomography*, Disease Markers, 19 (2003), pp. 107–121.

[50] D. Hall, G. Ma, F. Lesage, and Y. Wang, *Simple time-domain optical method for estimating the depth and concentration of a fluorescent inclusion in a turbid medium*, Opt. Lett., 29 (2004), pp. 2258–2260.

[51] M. Haltmeier, *Inversion formulas for a cylindrical Radon transform*, SIAM J. Imag. Sci., 4 (2011), pp. 789–806.

[52] M. Haltmeier, O. Scherzer, P. Burgholzer, and G. Paltauf, *Thermoacoustic computed tomography with large planer receivers*, Inverse Problems, 20 (2004), pp. 1663–1673.

[53] M. Haltmeier, T. Schuster, and O. Scherzer, *Filtered backprojection for thermoacoustic computed tomography in spherical geometry*, Math. Methods Appl. Sci., 28 (2005), pp. 1919–1937.

[54] L. Hervé, A. Koenig, and J.-M. Dinten, *Non-uniqueness in fluorescence-enhanced continuous wave diffuse optical tomography*, J. Opt., 13 (2011). 015702.

[55] R. W. Holt, K. M. Tichauer, H. Dehghani, B. W. Pogue, and F. Leblond, *Multiple-gate time domain diffuse fluorescence tomography allows more sparse tissue sampling without compromising image quality*, Opt. Lett., 37 (2012), pp. 2559–2561.

[56] Y. Hristova, *Time reversal in thermoacoustic tomography - an error estimate*, Inverse Problems, 25 (2009). 055008.

[57] Y. Hristova, P. Kuchment, and L. Nguyen, *Reconstruction and time reversal in thermoacoustic tomography in acoustically homogeneous and inhomogeneous media*, Inverse Problems, 24 (2008). 055006.

[58] H. Jiang, *Frequency-domain fluorescent diffusion tomography: a finite-element-based algorithm and simulations*, Appl. Opt., 37 (1998), pp. 5337–5343.

[59] A. Joshi, J. C. Rasmussen, E. M. Sevick-Muraca, T. A. Wareing, and J. McGhee, *Radiative transport-based frequency-domain fluorescence tomography*, Phys. Med. Biol., 53 (2008), pp. 2069–2088.

[60] H. K. Kim, M. Flexman, D. J. Yamashiro, J. J. Kandel, and A. H. Hielscher, *PDE-constrained multispectral imaging of tissue chromophores with the equation of radiative transfer*, Biomedical Optics Express, 1 (2010), pp. 812–824.

[61] A. Kirsch and O. Scherzer, *Simultaneous reconstructions of absorption density and wave speed with photoacoustic measurements*, arXiv:1109.5795, (2011).

[62] A. D. Klose and A. H. Hielscher, *Fluorescence tomography with simulated data based on the equation of radiative transfer*, Opt. Lett., 28 (2003), pp. 1019–1021.

[63] P. Kuchment, *Mathematics of hybrid imaging. a brief review*, in The Mathematical Legacy of Leon Ehrenpreis, I. Sabadini and D. Struppa, eds., Springer-Verlag, 2012.

[64] P. Kuchment and L. Kunyansky, *Mathematics of thermoacoustic tomography*, Euro. J. Appl. Math., 19 (2008), pp. 191–224.

[65] ——, *Mathematics of thermoacoustic and photoacoustic tomography*, in Handbook of Mathematical Methods in Imaging, O. Scherzer, ed., Springer-Verlag, 2010, pp. 817–866.

[66] P. Kuchment and D. Steinhauer, *Stabilizing inverse problems by internal data*, Inverse Problems, 28 (2012).

[67] A. T. N. Kumar, S. B. Raymond, B. J. Bacskai, and D. A. Boas, *Comparison of frequency-domain and time-domain fluorescence lifetime tomography*, Opt. Lett., 33 (2008), pp. 470–472.

[68] A. T. N. Kumar, S. B. Raymond, G. Boverman, D. A. Boas, and B. J. Bacskai, *Time resolved fluorescence tomography of turbid media based on lifetime contrast*, Optics Express, 14 (2006), pp. 12255–12270.

[69] L. Kunyansky, *Explicit inversion formulae for the spherical mean Radon transform*, Inverse Problems, 23 (2007), pp. 373–383.

[70] O. A. Ladyzhenskaya, *The Boundary Value Problems of Mathematical Physics*, Springer-Verlag, New York, 1985.

[71] J. R. Lakowicz, *Principles of Fluorescence Spectroscopy*, Plenum Press, New York, 1983.

[72] J. Laufer, B. T. Cox, E. Zhang, and P. Beard, *Quantitative determination of chromophore concentrations from 2d photoacoustic images using a nonlinear model-based inversion scheme*, Applied Optics, 49 (2010), pp. 1219–1233.

[73] F. Leblond, H. Dehghani, D. Kepshire, and B. W. Pogue, *Early-photon fluorescence tomography: spatial resolution improvements and noise stability considerations*, J. Opt. Soc. Am. A, 26 (2009), p. 1444.

[74] C. Li and L. Wang, *Photoacoustic tomography and sensing in biomedicine*, Phys. Med. Biol., 54 (2009), pp. R59–R97.

[75] X. D. Li, D. A. O'Leary, M. A. Boas, B. Chance, and A. G. Yodh, *Fluorescence diffuse photon density waves in homogeneous and heterogeneous turbid media: analytic solutions and applications*, Applied Optics, 35 (1996), pp. 3746–3758.

[76] Y. Lin, H. Gao, O. Nalcioglu, and G. Gulsen, *Fluorescence diffuse optical tomography with functional and anatomical a priori information: feasibility study*, Phys. Med. Biol., 52 (2007), pp. 5569–5585.

[77] Y. Lin, T. C. Kwong, G. Gulsen, and L. Bolisay, *Temperature-modulated fluorescence tomography based on both concentration and lifetime contrast*, J. Biomed. Opt., 17 (2012). 056007.

[78] A. V. Mamonov and K. Ren, *Quantitative photoacoustic imaging in radiative transport regime*, Comm. Math. Sci., (2012).

[79] R. H. Mayer, J. S. Reynolds, and E. M. Sevick-Muraca, *Measurement of fluorescence lifetime in scattering media using frequency-domain photon migration*, Appl. Optics, 38 (1999), pp. 4930–4938.

[80] W. McLean, *Strongly Elliptic Systems and Boundary Integral Equations*, Cambridge University Press, Cambridge, 2000.

[81] A. B. Milstein, J. J. Stott, S. Oh, D. A. Boas, and R. P. Millane, *Fluorescence optical diffusion tomography using multiple-frequency data*, J. Opt. Soc. Am. A, 21 (2004), p. 1035.

[82] W. Mo, D. Rohrbach, and U. Sunar, *Imaging a photodynamic therapy photosensitizer in vivo with a time-gated fluorescence tomography system*, J. Biomed. Opt., 17 (2012). 071306.

[83] F. Natterer, *Photo-acoustic inversion in convex domains*, Inverse Problems and Imaging, 6 (2012), pp. 315–320.

[84] L. V. Nguyen, *A family of inversion formulas in thermoacoustic tomography*, Inverse Probl. Imaging, 3 (2009), pp. 649–675.

[85] M. Niedre and V. Ntziachristos, *Comparison of fluorescence tomographic imaging in mice with early-arriving and quasi-continuous-wave photons*, Opt. Lett., 35 (2010), pp. 369–371.

[86] J. Nocedal and S. J. Wright, *Numerical Optimization*, Springer-Verlag, New York, 1999.

[87] V. Ntziachristos, *Fluorescence molecular imaging*, Annu. Rev. Biomed. Eng., 8 (2006), pp. 1–33.

[88] V. Ntziachristos, J. Ripoll, L. Wang, and R. Weissleder, *Looking and listening to light: the evolution of whole-body photonic imaging*, Nature Biotechnol., 23 (2005), pp. 313–320.

[89] M. O'Leary, D. Boas, X. Li, B. Chance, and A. Yodh, *Fluorescence lifetime imaging in turbid media*, Opt. Lett., 21 (1996), pp. 158–160.

[90] G. Paltauf, R. Nuster, M. Haltmeier, and P. Burgholzer, *Experimental evaluation of reconstruction algorithms for limited view photoacoustic tomography with line detectors*, Inverse Problems, 23 (2007), pp. S81–S94.

[91] G. Y. Panasyuk, Z.-M. Wang, J. C. Schotland, and V. A. Markel, *Fluorescent optical tomography with large data sets*, Opt. Lett., 33 (2008), pp. 1744–1746.

[92] S. K. Patch and O. Scherzer, *Photo- and thermo- acoustic imaging*, Inverse Problems, 23 (2007), pp. S1–S10.

[93] J. Qian, P. Stefanov, G. Uhlmann, and H. Zhao, *An efficient Neumann-series based algorithm for thermoacoustic and photoacoustic tomography with variable sound speed*, SIAM J. Imaging Sci., 4 (2011), pp. 850–883.

[94] E. T. Quinto, *Helgason's support theorem and spherical Radon transforms*, Contemporary Mathematics, 464 (2008), pp. 249–264.

[95] D. Razansky, M. Distel, C. Vinegoni, R. Ma, N. Perrimon, R. W. Köster, and V. Ntziachristos, *Multispectral opto-acoustic tomography of deep-seated fluorescent proteins in vivo*, Nature Photonics, 3 (2009), pp. 412–417.

[96] D. Razansky and V. Ntziachristos, *Hybrid photoacoustic fluorescence molecular tomography using finite-element-based inversion*, Med. Phys., 34 (2007), pp. 4293–4301.

[97] D. Razansky, C. Vinegoni, and V. Ntziachristos, *Multispectral photoacoustic imaging of fluorochromes in small animals*, Optics Lett., 32 (2007), pp. 2891–2893.

[98] K. Ren, G. Bal, and A. H. Hielscher, *Frequency domain optical tomography based on the equation of radiative transfer*, SIAM J. Sci. Comput., 28 (2006), pp. 1463–1489.

[99] K. Ren, H. Gao, and H. Zhao, *A hybrid reconstruction method for quantitative photoacoustic imaging*, SIAM J. Imag. Sci., 6 (2013), pp. 32–55.

[100] J. Ripoll and V. Ntziachristos, *Quantitative point source photoacoustic inversion formulas for scattering and absorbing media*, Phys. Rev. E, 71 (2005). 031912.

[101] A. Rosenthal, D. Razansky, and V. Ntziachristos, *Fast semi-analytical model-based acoustic inversion for quantitative optoacoustic tomography*, IEEE TRANSACTIONS ON MEDICAL IMAGING, 29 (2010), pp. 1275–1285.

[102] T. J. Rudge, V. Y. Soloviev, and S. R. Arridge, *Fast image reconstruction in fluorescence optical tomography using data compression*, Opt. Lett., 35 (2010), p. 763765.

[103] P. Shao, B. Cox, and R. J. Zemp, *Estimating optical absorption, scattering, and Grueneisen distributions with multiple-illumination photoacoustic tomography*, Appl. Opt., 50 (2011), pp. 3145–3154.

[104] V. Y. Soloviev, C. D'Andrea, M. Brambilla, G. Valentini, R. B. Schulz, R. Cubeddu, and S. R. Arridge, *Adjoint time domain method for fluorescent imaging in turbid media*, Applied Optics, 47 (2008), pp. 2303–2311.

[105] V. Y. Soloviev, K. B. Tahir, J. McGinty, D. S. Elson, M. A. A. Neil, P. M. W. French, and S. R. Arridge, *Fluorescence lifetime imaging by using time gated data acquisition*, Applied Optics, 46 (2007), pp. 7384–7391.

[106] P. Stefanov and G. Uhlmann, *Thermoacoustic tomography with variable sound speed*, Inverse Problems, 25 (2009). 075011.

[107] ——, *Thermoacoustic tomography arising in brain imaging*, Inverse Problems, 27 (2011). 045004.

[108] ——, *Recovery of a source term or a speed with one measurement and applications*, Transactions AMS, (2012).

[109] D. Steinhauer, *A reconstruction procedure for thermoacoustic tomography in the case of limited boundary data*, arXiv:0905.2954, (2009).

[110] ——, *A uniqueness theorem for thermoacoustic tomography in the case of limited boundary data*, arXiv:0902.2838v2, (2009).

[111] B. E. Treeby, E. Z. Zhang, and B. T. Cox, *Photoacoustic tomography in absorbing acoustic media using time reversal*, Inverse Problems, 26 (2010). 115003.

[112] V. Venugopal, J. Chen, F. Lesage, and X. Intes, *Full-field time-resolved fluorescence tomography of small animals*, Opt. Lett., 35 (2010), pp. 3189–3191.

[113] B. Wang, Q. Zhao, N. M. Barkey, D. L. Morse, and H. Jiang, *Photoacoustic tomography and fluorescence molecular tomography: A comparative study based on indocyanine green*, Med. Phys., 39 (2012), pp. 2512–2517.

[114] L. V. Wang, *Tutorial on photoacoustic microscopy and computed tomography*, IEEE J. Sel. Topics Quantum Electron., 14 (2008), pp. 171–179.

[115] L. V. Wang and S. Hu, *Photoacoustic tomography: In vivo imaging from organelles to organs*, Science, 335 (2012), pp. 1458–1462.

[116] Y. Wang, K. Maslov, C. Kim, S. Hu, and L. V. Wang, *Integrated photoacoustic and fluorescence confocal microscopy*, IEEE Trans. Biomed. Eng., 57 (2010), pp. 2576–2578.

[117] M. Xu and L. Wang, *Universal back-projection algorithm for photoacoustic computed tomography*, Phys. Rev. E, 71 (2005). 016706.

[118] M. Xu and L. V. Wang, *Photoacoustic imaging in biomedicine*, Rev. Sci. Instr., 77 (2006). 041101.

[119] Y. Xu, D. Feng, and L. V. Wang, *Exact frequency-domain reconstruction for thermoacoustic tomography. i. planar geometry*, Medical Imaging, IEEE Transactions, 21 (2002), pp. 823–828.

[120] Y. Xu, M. Xu, and L. V. Wang, *Exact frequency-domain reconstruction for thermoacoustic tomography. ii. cylindrical geometry*, Medical Imaging, IEEE Transactions, 21 (2002), pp. 829–833.

[121] Z. Yuan and H. Jiang, *Simultaneous recovery of tissue physiological and acoustic properties and the criteria for wavelength selection in multispectral photoacoustic tomography*, Optics Letters, 34 (2009), pp. 1714–1716.

[122] A. D. Zacharopoulos, P. Svenmarker, J. Axelsson, M. Schweiger, S. R. Arridge, and S. Andersson-Engels, *A matrix-free algorithm for multiple wavelength fluorescence tomography*, Optics Express, 17 (2009), pp. 3025–3035.

[123] R. J. Zemp, *Quantitative photoacoustic tomography with multiple optical sources*, Applied Optics, 49 (2010), pp. 3566–3572.

[124] W. P. Ziemer, *Weakly Differentiable Functions : Sobolev Spaces and Functions of Bounded Variation*, Springer-Verlag, New York, 1989.